# Position-independent refinement of vagus motor neuron wiring

Takuya Kaneko[1, 4], Jonathan Boulanger-Weill[2], Adam J Isabella[1, 3], Cecilia B Moens[1,4]

[1]Division of Basic Sciences, Fred Hutchinson Cancer Center, Seattle, Washington 98109, USA

[2]Department of Molecular and Cellular Biology, Faculty of Arts and Sciences, Harvard University, Cambridge, MA 02138, USA; Center for Brain Science, Faculty of Arts and Sciences, Harvard University, Cambridge, MA 02138, USA; Sorbonne Université, Institut National de la Santé et de la Recherche Médicale, Centre National de la Recherche Scientifique, Institut de la Vision, Paris, France

[3]Department of Genetics, Cell Biology, and Development, University of Minnesota, Minneapolis, Minnesota 55455, USA

[4]Corresponding authors (tkaneko@fredhutch.org, cmoens@fredhutch.org)

**ABSTRACT**

The vagus nerve (10th cranial nerve) mediates brain-body communication by innervating and controlling various internal body parts, including the pharynx, larynx, and most visceral organs. Vagus sensory neurons send information about internal states to the brain, and vagus motor neurons return reflexive motor responses, such as gagging, swallowing, digestive enzyme secretion, gut peristalsis and heart rate adjustment. The diverse motor neurons underlying these bodily functions are topographically organized in the brainstem. However, the topographic map is continuous, with motor neurons innervating a common target, a "target group", partly intermingled with neurons of other target groups, without clear boundaries. Particularly, motor neurons supplying different pharyngeal muscles are significantly overlapping in the topographic map throughout vertebrates. It remains unanswered how this intermingled diverse population of motor neurons can control different bodily functions. Through calcium imaging in larval zebrafish, we demonstrate that, when noxious stimulation is given focally to the larval pharynx, vagus motor neurons return stereotypic muscle activity patterns appropriate for the location of the stimulus. We show that vagus motor neurons that produce pharyngeal contraction following focal noxious stimulation are loosely distributed in the motor nucleus, consistent with the loose and overlapping distribution of anatomical target groups. This suggests that the connectivity of motor neurons is determined at the single-neuron level, not the neighboring population level. Remarkably, we show that pharynx-innervating motor neurons can maintain their appropriate response patterns to focal noxious stimulation even when their topographic organization is disrupted, and that mis-positioned motor neurons elaborate dendrites that extend towards the dendritic territory of their target group. We further identified that the motor activity patten is immature when motor neurons first initiate sensory-evoked responses and that maturation, dendrite extension and incorporation into the correct sensory motor circuit all depend on the efficiency of neurotransmission from the motor axons. Our data together suggest a position-independent wiring strategy that refines presynaptic connectivity of motor neurons through experience-dependent feedback regulation. We further demonstrate resilience to topographic manipulation in viscera-innervating vagus motor neurons, supporting that position-independent wiring is a general principle.

## INTRODUCTION

Just as it interacts with the external world around us, so our brain interacts with the internal world within us – our internal body parts – through sensory circuits that monitor body physiology and motor circuits that return necessary bodily functions on demand. A major mediator of brain-body communication is the 10$^{th}$ cranial nerve, the vagus[1,2], which innervates a wide array of body parts including the pharynx, larynx and most visceral organs in vertebrates. Vagus sensory afferents send information about diverse aspects of internal state to the brain, and in turn, vagus motor efferents transmit appropriate reflexive motor responses including coughing, gagging, swallowing, esophagus and gut peristalsis, stomach emptying, heart rate and pancreatic and gall bladder secretion[1-4].

Given the range of muscles and organs innervated by the vagus nerve, it is surprising that all the vagus efferents continuously lie in two motor nuclei in the brainstem in mammals (the dorsal nucleus, DMV and the nucleus ambiguus, nAmb) or a single motor nucleus in fish, with imperfect anatomical separation between neurons that innervate different targets[5,6] . Vagus motor neurons with different targets exhibit a coarse scale of topographic organization within the motor nucleus[7-9]. For example, pharynx contracting neurons lie in the semi-loose compartment of the mAmb, anterior to larynx contracting neurons in the loose compartment[7,] and stomach contracting neurons in the DMV generally lie anterior to stomach relaxing neurons [10], though with significant spatial overlap. In the zebrafish we have previously described a topographic relationship between vagus motor neurons and their targets whereby more anterior neurons in the vagus motor nucleus innervate more anterior pharyngeal arch-derived muscles and more posterior neurons innervate more posterior pharyngeal arches and the viscera, and we discovered the developmental mechanism by which this topographic relationship is established[6,11,12]. However, in all these cases of topographic mapping by vagus motor neurons in mammals and fish, groups of motor neurons innervating the same body target are loosely distributed and extensively intermingled with different groups[7,9,11,12] Significant overlap is particularly evident among neurons innervating different muscles in the pharynx[13], which are also mixed with heart-innervating neurons in mammals[14]. This is unlike in the spinal cord, where the motor neurons that innervate specific limb muscles are clustered in distinct motor pools[15-18].

How are these intermingled diverse motor neurons incorporated in neural networks? A positional strategy such as occurs in limb-innervating motor neurons, where the position of motor neurons determines which presynaptic neurons they connect to[19-22], would likely cause neighboring vagus motor neurons to connect with common presynaptic neurons, making functionally heterogenous groups of neurons fire together. It is an open question whether, and how, adjacent neurons with different functions can be activated differently for sophisticated peripheral control. Understanding the wiring strategy of vagus motor neurons is necessary because dysfunction in motor wiring can result in adverse conditions such as defective swallowing (dysphagia)[23,24] and non-specific baroreflex or pulmonary reflex recruitment during swallowing or gagging[25-27].

In this study, we establish the zebrafish as a tractable model for investigating motor wiring of the vagus. By 3 days of embryonic development its single vagus motor nucleus contains diverse neurons that innervate the pharyngeal arches and viscera[6,28]. Zebrafish embryos are amenable to a wide variety of experimental manipulations. In particular, our recent studies developed methods to manipulate topographic positioning of vagus motor neurons to determine the timing and mechanism of axonal targeting[12,28]. Furthermore, zebrafish embryos and larvae are amenable to the live imaging of neuronal activity evoked by sensory stimuli, allowing us to study functional aspects of vagus connectivity. This gives us the opportunity to examine the contribution of the positional strategy in vagus motor wiring.

Here we report that vagus motor neurons that are activated by sensory stimulation to the pharynx and gastrointestinal tract are not clustered together but are loosely distributed, consistent with the loose distribution of anatomical target groups. Through the unclustered activity pattern, vagus motor neurons achieve differential control of different body parts, appropriate for a given sensory stimulation. This suggests that the connectivity of motor neurons is determined at the single-neuron level, not the neighboring population level. Remarkably, the motor activity pattern providing sophisticated body control is resilient to disrupted topographic organization, supporting a position-independent strategy for refining sensorimotor connectivity in a continuous topographic map. We further demonstrate that the motor activity pattern is influenced by the relative efficacy of neurotransmission from the motor axons, which argues experience-dependent regulation mediated by periphery-to-brain feedback signaling. This study reveals a novel motor wiring strategy utilized by intermingling vagus motor populations.

## RESULTS

### Vagus motor neurons with distinct functions are mixed in the brainstem

After projecting from the brainstem as a single fascicle, the vagus motor nerve splits into five major branches in the periphery (Fig. 1a,b)[11,12]. The first three branches innervate muscles of pharyngeal arches 4-6 for swallowing and gill opening and closing (branches 4-6) (Fig. 2a). Hereafter, we collectively call neurons in these three “pharyngeal branches” as “pharynx-targeting neurons”. In some fish, these neurons control a complex intra-oral food sorting behavior that separates the edible components from detritus and regurgitates the inedible parts through a 3-neuron reflex circuit (sensory>interneuron>motor)[29,30] . The fourth branch innervates the chewing muscles of the pharyngeal tooth-bearing pharyngeal arch 7, and the fifth branch projects towards the viscera where it branches further to provide pre-synaptic parasympathetic innervation to the organs (branch v in Fig. 2a). Individual vagus motor neurons only innervate a single branch and once an axon selects a branch it does not change[11,12]. We refer to the group of motor neurons that innervate an individual branch of the vagus nerve as a "target group”.

The five target groups are topographically organized along the anterior-posterior (A-P) extent of the nucleus, reflecting the A-P organization of the five branches (Fig. 1b)[11,12]. However within this branch-level topography, motor neurons are continuously mapped with no morphological boundary between target groups (Fig.1b, c). In particular, the three target groups constituting pharynx-innervating branches PA4-6, visualized by the sequential photoconversion and imaging of individual branches in a single Tg(isl1:Kaede)[31] fish, are highly intermingled within the anterior third of the nucleus, so that neurons from adjacent target groups are frequently positioned at the same A-P level (Fig. 1c). Likewise, viscera-targeting neurons occupy the posterior end of the nucleus; but there is no apparent morphological distinction between neurons that innervate different organs, analogous to the continuous topography of the mammalian DMV (Fig. 1b, c, h)[9]. Lastly, neurons that innervate branch 7 are widely scattered along the A-P extent of the nucleus (Fig 1b, c, g). Thus, as in mammals, the vagus motor nucleus lacks motor pool organization, and motor neurons can be adjacent to or even surrounded by neurons from different target groups.

Similarly, motor dendrites, which develop after the motor axon selects a single branch, extend longitudinally in a neuropil ventral to the motor nucleus and have an overlapping, continuous topographic organization with no morphological distinction between the dendrites of different target groups (Fig.1d-h). The spatial overlap is particularly evident amongst the dendrites of pharynx-targeting neurons (Fig. 1d-f, S1). These observations are consistent with a study in the mammalian nAmb reporting a significant spatial overlap between motor neurons innervating different pharyngeal muscles[13] and the lack of unique dendritic morphology amongst neighboring motor neurons[7,32], and therefore predicts that there may be a conserved strategy for wiring pharynx-controlling motor neurons across vertebrates.

### Functional topography of vagus motor responses to spatially distinct sensory cues

To begin investigating wiring of spatially mixed pharynx-targeting neurons, we first examined whether different pharyngeal muscles can be differently controlled despite the spatial overlap between the motor neurons that innervate them. We aimed at inducing motor responses from pharyngeal muscles by delivering noxious stimulation to the pharynx of 10-11 day post-fertilization (dpf) larval zebrafish with optovin, a photo-activatable ligand for TrpA1 nociceptive channels [33]. Focal UV illumination over the pharynx locally activates optovin and stimulates TrpA1b expressing vagus sensory neurons in the nodose and epibranchial ganglia (Fig. S2a-e). Focal UV illumination of the pharynx in the presence of optovin induces reflexive muscle contraction that may be analagous to the gag reflex which mammals and fish use to expel inedible materials from the pharynx[29,30] (Movie 1).

Importantly, by driving GCaMP6s expression in pharyngeal muscles with *tcf21*$^{Gal4}$*;* Tg(UAS:GCaMP6s)[34], we observed that, although focal noxious stimulation often induces responses from all of the PA4, PA5, and PA6 muscles, the relative level is different. Focal noxious stimulation of the anterior pharynx (between PA3 and PA4) induces a stronger response in the PA4 muscle, near the stimulation spot, than in the PA5 and PA6 muscles (Fig. 2a-d). In contrast, focal stimulation of the posterior pharynx (between PA6 and PA7) induces a stronger response in the nearby PA5 and PA6 muscles than the more distant PA4 muscle (Fig. 2a-d). The muscle response is dependent on the presence of optovin (Fig. 2d). Stronger muscle responses near the noxious cue might be a strategy to effectively expel potentially dangerous items in the pharynx. We quantified the difference in calcium responses to the two pharyngeal stimulations as “tuning” in which an exclusive response to anterior pharynx stimulus is a "tuning index” score of 1 and exclusive response to a posterior stimulus is a score of 0 (Fig. 2e). The anterior PA4 muscle and the posterior PA5, PA6 muscles exihibit tuning differences, which are stereotypic across animals. Thus, in spite of extensive overlap of motor dendrites, pharynx-targeting motor neurons are able to control individual pharyngeal muscles differently, generating muscle contraction patterns along the A-P axis, corresponding to the position of the noxious stimulus.

To directly assess activities in vagus motor neurons underlying stereotypic pharyngeal constriction, we imaged GCaMP signals in the motor axon branches innervating PA4, 5, and 6 in 10-11 dpf Tg(chata:Gal4; UAS:GCaMP6s) larvae in response to focal noxious stimulation mediated by optovin as above (Fig. 2f). As expected from the activity patterns in pharyngeal muscles, we find that anterior pharynx stimulation robustly activates the PA4 branch with weaker activity from PA5 and PA6 branches, while posterior pharynx stimulation strongly activates PA5 and PA6 branches with weaker activity from the PA4 branch (Fig. 2f-h). Each animal shows the same patterns of axonal activities following repeated delivery of sensory cues, and the responses are stereotyped with little variation across different zebrafish larvae (Fig. 2g,h). This results in a tuning difference among the three axonal branches, which is indicative of *functional topography* (Fig. 2l, right panel) because it represents functional segregation amongst the neurons innervating them. From this observation, we infer that pharnx-targeting motor neurons are tightly connected with upstream sensory circuits responsible for detecting stimuli in the same anatomical region. Thus, our finding predicts that

since they cannot change their output (i.e., axonal) connectivity, motor neurons at the same A-P position on the topographic map develop different input (i.e., somatodendritic) connectivity for sophisticated motor control in the periphery.

**Functional topography emerges after vagus motor axon targets are fixed**

We find that the functional topography we identified from axonal imaging is immature in younger larvae. Vagus motor neurons show sensory-evoked activity as early as 4 dpf, shortly before larval zebrafish begin eating. But, at this stage, focal noxious stimulation delivered as above induces similar activity levels in all three branches (PA4-PA6; Fig. 2i-l). Axonal activities exhibit immature functional topography with all three branches showing a tuning index close to 0.5 (Fig. 2l, left panel). At 7dpf, tuning differences are more evident but still less mature than that at 10-11 dpf (Fig. 2l, middle vs right panel). This finding is unexpected, given that the topographic organization of motor neurons that we have described is already established at 3 dpf with no subsequent change in axonal targeting detected (Fig 1a,b)[11,12]. Thus our data support a model where input connectivity of vagus motor dendrites is progressively fine-tuned for more sophisticated peripheral control after motor neurons begin producing motor outputs.

To map the A-P distribution of responding neurons on the continuous topographic map, we expressed nuclear GCaMP6s in motor neurons (Tg(isl1:H2B-GCaMP6s)) and imaged a single focal plane of the vagus motor nucleus during focal noxious stimulation (Fig. 3a). At 10-11 dpf vagus motor neurons that respond repeatedly to repeated noxious stimulation to the pharynx (either anterior or posterior pharynx) are localized to the anterior ~30 µm of the ~150 µm long motor nucleus, with no or little response from more posterior neurons (Fig. 3a-c). This is a smaller region than the area occupied by pharynx-targeting neurons (~45 µm) (Fig. 1c-f), indicating that only a subset responds to contract pharyngeal muscles. Although repeated noxious stimulation to the same pharyngeal location does not always activate the exact same motor population, the pattern is highly correlated (Fig. 3f). This observation suggests that pharyngeal noxious inputs selectively induce pharyngeal motor outputs without significantly affecting other body parts under vagal control. This anterior-localized response pattern is not reproduced by esophagus noxious stimulation, which typically involves calcium responses in posterior-most motor neurons together with a subset of anterior neurons (Fig. 3a,b). Thus, selective control of the pharynx is a unique output specifically induced by noxious cues in the pharynx.

However, within the anterior region of the nucleus, motor neurons responding to pharyngeal stimulations are not spatially clustered, but instead loosely distributed. Responding neurons are often surrounded by non-responding neurons (Fig. 3a) at the same A-P position with non-responders (Fig. 3d). Such salt-and-pepper activity patterns within the anterior region are induced by both anterior and posterior pharyngeal stimulation with no noticeable difference in the A-P distribution of responding neurons, though fewer neurons responded to the anterior stimulation in the imaging focal plane (Fig. 3c,d). We detected only a small number of neurons that responded exclusively to one stimulation (Fig. 3a-c), which is in agreement with our observation above that pharyngeal axonal branches usually respond to both anterior and

posterior pharyngeal stimulation, though with different activity levels (Fig 1c-f). Consistently, we found that neurons with different tuning preference to the two stimulations are intermingled, with most tuned toward posterior stimulation to varying degrees (Fig. 3e). This spatially disorganized activity pattern is not due to stochasticity in each response, because repeated stimulation to the same spot in a given fish induces more correlated activity patterns than stimulation to different spots does (Fig.3f), thus likely reflecting loose distribution of target groups. The lack of synchronized activity in neighboring motor neurons indicates that stereotyped motor axon responses and muscle contraction in the pharynx is established by fine-scale connection specificty that differently wires neighboring vagus motor neurons at the same A-P position.

As we expected from the immature axonal activity patterns we observed in 4 dpf larvae, the motor nucleus displays immature response patterns at this early stage as well. Overall a much higher proportion of vagus motor neurons respond at 4 dpf compared to 10-11 dpf, and the response is much broader, sometimes including the posterior region of the nucleus where viscera-targeting motor neurons reside (Fig. 3g-i). Thus, although the anterior-posterior motor topography is established by 3 dpf, input connectivity is dispersed and immature. Within the anterior region, neighboring neurons often respond synchronously with few non-responding neurons intermingled (Fig. 3g,j). In addition, a large proportion of neurons respond with similar levels to anterior and posterior pharynx stimulation, consistent with the immature tuning we observed from axonal imaging (Fig. 3k). Thus, the response pattern of vagus motor neurons to noxious inputs changes after their initial spatial organization is established by 3 dpf.

We asked whether these developmental changes in motor responses to noxious inputs could be attributable to possible changes in the upstream nociceptive sensory pathway. Trpa1b-expressing sensory neurons, whose cell bodies reside in the nodose and epibranchial ganglia, transmit optovin-derived noxious cues from the pharynx to the brainstem, where their axon terminals are arranged topographically dorsal to the motor dendritic neuropil (Fig. S2a,b,f). As with vagus motor neurons and motor dendrites, the axons of sensory neurons innervating anterior PAs terminate anteriorly to those of neurons innervating posterior PAs, with a significant degree of spatial overlap (Fig. S2f). We expressed GCaMP6s in Trpa1b sensory neurons with Tg(*TrpA1b*$^{Gal4}$*; UAS:GCaMP6s*), and we studied, from 7 dpf larvae, the neuronal and axonal calcium responses to anterior and posterior pharyngeal and esophageal noxious stimulation, as above. At the level of sensory neuron cell bodies, anterior and posterior pharyngeal stimulation activated distinct Trpa1b-expressing sensory neurons (Fig. S2c-e). At the level of central sensory processes, we identified topographically organized activity patterns, with progressively more posterior stimuli exciting progressively more posterior sensory processes (Fig. S2g-i). Importantly, this pattern is already evident in 4 dpf larvae and remains unchanged in 10 dpf larvae (Fig. S2i). Although these experiments cannot rule out fine-scale changes in sensory neuron synapse organization over time or changes in the central circuit organization, they are consistent with a model in which the maturation of the motor response between 4 dpf and 10 dpf is driven by progressive refinement in the input connectivity of motor neurons.

**Functional topography can be established independent of motor neuron position**

Our data so far has demonstrated that motor neurons with different response patterns are mixed at the same A-P position of the vagus motor nucleus and that this spatially disorganized activity pattern inside the anterior portion of the nucleus generates stereotyped axonal activity patterns in the periphery in 10-11 dpf larvae. These findings support the idea that individual motor neurons develop specific input connectivity that is appropriate for their innervation targets, independent of their positioning, contrary to the positional strategy used in spinal motor neurons[19,20]. However, it remains possible that some cryptic spatial organization exists among pharynx-targeting neurons to provide stereotypic axonal activity in the pharnx. To directly test this possiblity, we sought to examine whether appropriate axonal activity is provided by pharynx-targeting neurons whose position is manipualted. We disrupted the topographic organization by transplanting neurons collected from various positions in the motor nucleus of a *Tg*(chata:Gal4, UAS:GCaMP6s, isl1:membRFP) donor embryo and placing them as a small cluster inside the anterior third of the vagus motor nucleus of a host embryo (Fig. 4a,b). We performed these transplants at 40 hpf, after donor pharynx-targeting neurons had already innervated their targets, so that they would regrow to a target consistent with their *original position* regardless of their *new position*[28]. This approach thus generated a GCaMP-expressing motor cluster in which diverse motor neurons are randomly positioned (Fig. 4b). To focus the motor response specifically onto the small number of transplanted motor neurons during calcium imaging, we silenced the host motor neurons, which maintain intact positioning, by genetically expressing the botulinum toxin light chain, or BoTxBLC-GFP, a specific inhibitor of neurotransmission release (see below for further explanation)[35]. Then we measured GCaMP responses of regenerated donor-derived axons in the pharyngeal branches at 10-11 dpf (Fig. 4c,d). Overall detected responses are weaker due to the small number of GCaMP-expressing donor-derived axons and some background GFP siganls derived from BoTxBLC-GFP expression. However, similar to what we saw in intact fish (Fig. 2f-h), anterior pharyngeal stimulation preferentially activates donor-derived axons in the PA4 branch and posterior stimulation robustly activates those in the PA5 and PA6 branches (Fig. 4c). Consequently functional topography is evident as in non-transplanted controls (Fig. 4d). Thus, even when topographic organization among pharynx-targeting neurons is absent, these neurons can develop specific input connectivity for stereotypical functional outputs to the pharynx.

To further investigate the ability of vagus motor neurons to develop specific input connectivity independent of neural positioning, we generated pharynx-targeting neurons physically distant from their normal position in the motor nucleus, surrounded by non-pharynx-targeting neurons, and examined their activity patterns. We turned again to the heterotopic transplantation paradigm described above in which donor-derived motor neurons regrow to their original targets[28], combined with calcium imaging of donor-derived neuron soma (Fig. 4e, i). Here again, to focus the motor response to the small number of donor-derived neurons, we inhibited neurotransmission from host motor neurons with BoTxBLC expression. We find that pharynx-innervating neurons transplanted to the middle of the motor nucleus, which regrow axons to PA4-PA6, respond to pharynx stimulation at 10-11 dpf (Fig. 4f,g,m,n), although motor neurons at this topographic position, which largely innervate PA7, rarely respond to pharyngeal

stimulation at this stage (Fig. 1g, Fig. 3c). This result suggests that pharynx-targeting neurons, even if displaced from their normal A-P position, can develop specific input connectivity that is appropriate for their output patterns. In contrast, viscera-innervating neurons transplanted to the same position, which do not regrow to the pharyngeal branch, do not respond to pharynx stimulation (Fig. 4j,k,m,n). Taken together, vagus motor neurons gain appropriate response patterns at the single cell level, independent of neural positioning.

**Mispositioned vagus motor neurons can adjust dendritic architecture**

What is the mechanism that enables transplanted neurons to integrate into functionally appropriate sensory-motor circuits? By studying the morphology of transplanted neurons after calcium imaging, we noted that transplanted neurons extend dendrites differently depending on where their axons innervate. Whereas the dendritic arbors of posterior-derived motor neurons preferentially extend posteriorly (Fig. 4l, o), those of anterior-derived pharynx-targeting motor neurons show relatively more anterior extension (Fig. 4h, o). This significant morphological difference between these two groups of transplanted neurons may contribute to the difference we observe in their activity patterns. This observation raised the possibility that dendrites of ectopic neurons can extend towards the neuropil occupied by the dendrites of their target group for correct input connectivity.

Similar dendritic adjustment was observed when topographically incorrect motor neurons were generated at the single cell level by an independent method. Individual vagus motor neurons that express a dominant-negative retinoic acid receptor (DN-RAR) innervate more anterior pharyngeal arch targets than non-expressing neurons at the same position, due to premature initiation of an axon guidance program[11]. We generated larvae with one or a few DN-RAR-expressing neurons per motor nucleus using Tg(isl1:Gal4; UAS:DN-RAR-p2A-GFP-CAAX). We observe that the dendrites of posteriorly located DN-RAR-expressing motor neurons, whose axons often innervate the pharynx, frequently extend far anteriorly toward the dendritic neuropil of endogenous pharynx-targeting neurons in 7-8 dpf larvae (Fig. 6a-d, g).

While this is a more dramatic adjustment than what would be needed for connectivity specification under normal circumstances where intermingled dendrites of adjacent target groups develop different synaptic inputs, it unveils a remarkable ability of motor neurons at the same A-P position to adjust input connectivity corresponding to their output target. Taken together, our findings reveal a novel motor wiring strategy that, contrary to the positional strategy, establishes specific input connectivity at the single cell level in a heterogeneous motor cluster.

**Both functional topography and dendritic adjustment depend on motor neuron output**

Next, we sought to investigate whether separate input connectivity to intermingled motor dendrites is established through experience-dependent adjustment. We considered this possibility because the fine-tuning of the vagus motor neuron response pattern correlates with

the onset of sensory-evoked motor activity (Fig. 2l). In fact, in many sensory systems, point-to-point connection specificity is established by animals' experience of sensory inputs[36-38]. In addition, experienced motor activity is reported to regulate synapse formation of motor neurons with their postsynaptic muscles in the *Drosophila* neuromuscular junction (NMJ)[39].

To determine the contribution of experience-dependent regulation, we suppressed the ability of vagus motor neuros to generate motor output through the inhibition of synaptic transmission. We expressed BoTxBLC, which blocks acetylcholine release [35], in motor neurons using the Gal4/UAS system (Tg(isl1:Gal4, UAS:BoTxBLC-GFP)). By combining calcium imaging of the vagus motor nucleus using Tg(isl1:H2B-GCaMP6s), we find that BoTx expression significantly reduces the number of anterior motor neurons that respond repeatedly to focal pharyngeal noxious stimulation at 10-11 dpf (Fig.6a-d). This effect is not due to defects in motor neuron physiology, because most BoTx+ neurons respond to intense noxious inputs given by bath application of allyl-isothiocyanate, a natural agonist of TrpA1 (Fig. 6b-d), and, variably and for unknown reasons, to optovin stimulation of the esophagus . We find no noticeable change in the topographic axonal projections or gross dendritic projection patterns in BoTx-expressing motor neurons (Fig. 6e,f). Thus, pharynx-targeting motor neurons, when their activities are ineffective in contracting pharyngeal muscles, become less responsive to pharyngeal noxious cues, supporting experience-dependent connectivity adjustment.

We find that this effect of BoTxBLC expression is cell-autonomous. When we generated non-BoTx-expressing pharynx-targeting motor neurons inside BoTx-expressing animals through transplantation (Fig. 6g-i)[12,28], these BoTx-negative neurons, whose neurotransmission is thus intact, are activated by focal pharyngeal noxious stimulation (Fig. 6h,j). Importantly, BoTx-negative neurons in BoTx-expressing animals show a significantly higher calcium response than they normally do in non-Botx-expressing animals (Fig. 6j). This response elevation in transplanted neurons possibly reflects a compensatory mechanism that helps generate normal pheripheral outputs from a small number of BoTx-negative functional motor neurons in otherwise Botx-expressing animals. Above we referred to this effect as "focusing the response on the transplanted neurons" and used it to facilitate our transplant approach, given the sparsity of repeatedly responding motor neurons under normal conditions (Fig. 3a).

The observation that the motor neurons that can most effectively transmit a signal are distinguished and strongly selected to participate in the circuit suggests the presence of a feedback signal that reinforces connectivity with upstream neurons at the single cell level. We suspect that the feedback signaling originates from postsynaptic targets, carries information about peripheral responses to localized sensory cues, and then adjusts motor connections with upstream neurons to optimize the accuracy of these responses. We hypothesize that this single-cell- level adjustment may be the same mechanism that enables motor neurons to become integrated into the correct circuit, independent of their nucleus positioning.

To test this hypothesis, we returned to the sparse DN-RAR expression method to generate posterior neurons that ectopically innervate PA4-6 as described above (Fig. 5a-d), but now

blocked neurotransmission by co-expressing BoTxBLC in the entire motor nucleus (isl1:Gal4; UAS:BoTxBLC-GFP). By imaging 7-8 dpf larvae, we found that neurons co-expressing DN-RAR and BoTxBLC successfully extend dendrites ventrally into the motor neuropil, but often they arborize locally, at the level of the cell body (Fig. 5e-g) similar to other posterior neurons that project appropriately to the viscera (Fig. 5b). We infer that in the absence of neurotransmission, this neuron was unable to identify upstream neurons that allow it to complete the sensorimotor circuit that would generate an appropriate response to pharynx stimulation in spite of its incorrect position. Taken together, our data argue that single-cell level connectivity adjustment that is needed for position-independent vagus motor wiring is mediated by neurotransmission-induced feedback signaling that reports peripheral motor performance back to the brain.

**Position-independent strategy is a general principle across diverse vagus motor neurons**

Our study so far has focused on the pharynx-targeting motor population due to substantial spatial overlap amongst target groups in the anterior part of the motor nucleus. As the last step of this study, we examined whether the position-independent circuit adjustment we identified above is a general principle across diverse vagus motor populations, by analyzing viscera-targeting motor neurons which lie in the posterior part of the motor nucleus and project in a single branch of the vagus nerve that further branches to regulate the functions of multiple visceral organs [12]. Similar to pharynx-targeting vagus motor neurons, viscera-targeting motor neurons have overlapping dendrites, presumably requiring fine-scale functional segregation for independent organ control.

Optovin-mediated noxious stimulation of the esophagus often involved activation of pharynx-targeting neurons together with viscera-targeting neurons (Fig. 3a,b). Hence, we developed a different method to induce activities from viscera-innervating vagus motor neurons. Vagus sensory neurons detect esophageal stretch caused by the presence of a bolus of food and induce a peristaltic reflex driven by esophagus-innervating vagus motor neurons [40] . We experimentally induced esophageal peristalsis by injecting a droplet of oil into the larval esophagus to mimic a bolus of food in 7-8 dpf larvae (Fig. 7a,b). Larvae respond to this stimulus with some latency by moving the injected oil to the stomach (Movie 2). Through calcium imaging with Tg(HuC:H2B-GCaMP6s), we found that larval zebrafish at 7-8 dpf can respond to this stimulus with high activities in posterior vagus motor neurons and little or no activity in anterior motor neurons (Movie 3), although we also observed activity in other neurons outside of the isl1:Kaede-expressing vagus motor nucleus, possibly reflecting the complexity of the swallowing response.

This selective posterior activation caused by inducing esophagus stretch provided us the opportunity to study the contribution of neural positioning to circuit wiring amongst viscera-targeting neurons. We asked whether viscera-innervating motor neurons misplaced in the anterior third (anterior 45 µm) of the nucleus, where pharynx-targeting neurons reside, show coordinated activity patterns with endogenous viscera innervating neurons, similar to how posteriorly misplaced pharynx-targeting motor neurons show similar activity patterns to their

distant target groups as we described above (Fig 4f,m,n). We generated ectopic viscera-targeting neurons through the sparse overexpression in anterior motor neurons of *hoxb5a*, which, we previously reported, is normally expressed only in posterior vagus motor neurons and can direct visceral axonal targeting when ectopically expressed in anterior neurons[12] (Fig.7c). To identify anterior viscera-targeting neurons induced by ectopic *hoxb5a* expression, we photoconverted the visceral branch of Tg(isl1:Kaede); Tg(isl1:Gal4); Tg(UAS:*hoxb5a*-p2A-GFP-CAAX); Tg(HuC:H2B-GCaMP6s) larvae and identified membrane-GFP-expressing neurons in the anterior part of the motor nucleus that were retrogradely labeled with Kaede$^{RED}$ (Fig. 7c-e). Then we photoconverted the entire motor nucleus to eliminate Kaede$^{GREEN}$ fluorescence and performed GCaMP6s imaging of a single plane including the ectopic viscera-innervating neurons while injecting oil into the esophagus. From 7-8 dpf larvae, we found that oil injections that induce a response in endogenous viscera-innervating motor neurons frequently activate ectopic viscera-targeting neurons in the anterior vagus motor nucleus (Fig. 7e (#1), 7g) (Movie 4). In these instances, the activity pattern of ectopic anterior neurons was more correlated with posterior motor neurons than with anterior motor neurons that surround them (Fig.7f,h), supporting that the activity pattern depends more on the axonal innervation pattern than the position of nucleus.

Taken together, our results show that both pharynx-targeting neurons and viscera-targeting neurons can be incorporated into correct circuits independent of their positions on the topographic map. While the limitations of the esophageal stretch experimental approach prevent us from asking whether this is an experience-dependent process involving dendritic re-targeting for viscera-innervating neurons like it is for pharynx-innervating neurons, our findings suggest that a position-independent strategy is a general principle across diverse vagus motor neuron target groups.

## DISCUSSION

This study unveiled a striking ability of vagus motor neurons to develop specific input connectivity that is appropriate for their innervation targets, independent of their position within the motor nucleus. Although vagus motor neurons that innervate different targets are spatially intermingled in the brain of larval zebrafish, they produce stereotyped peripheral outputs that differently regulate these different targets. We demonstrate remarkable resilience of input connectivity to manipulations that alter motor neuron positions and identified a single-neuron-level adaptive dendritic extension as one plausible mechanism. We additionally provide evidence that specific input connectivity is in part established by neurotransmission-mediated feedback from the periphery, supporting experience-dependent regulation. This study has established a tractable zebrafish model for investigating mechanistic insights into vagus motor wiring.

### Position-independent motor wiring

Our findings in the vagus system contrast with well-studied spinal motor circuits in which motor neurons innervating different muscles are separated into spatially discrete motor pools that receive monosynaptic input from sensory neurons innervating the same muscle based on their position in the spinal cord[41,42]. Genetic manipulations that change the motor pool organization result in mis-wiring and consequent motor behavior defects[22]. We previously showed that vagus motor neurons have a topographic relationship with their peripheral targets and hypothesized that this relationship serves to position motor neurons optimally to receive sensory input from the same body regions[11,12]. However the lack of motor pool organization within the vagus motor nucleus predicts that a simple positional mechanism is insufficient to generate such precise connectivity. Our identification of the resilience of vagus motor neurons to topographic defects, which we have described at the single-cell level, provides direct evidence that the connectivity of this motor population is indeed specified differently. However, we note that only about a half of mis-positioned neurons exhibits correlated activity with distant neurons of the same target group (non-responders in Fig7g,h), or generate adaptive dendritic projections (Fig. 5g), suggesting that optimal responses depend on a combination of neuron position and subsequent connectivity refinement.

Since mammalian vagus motor neurons innervating different targets are also highly intermingled[7,10,13,32,43] we speculate that in mammals too, vagus motor neurons may adjust their connections to presynaptic neurons to fire differently from adjacent neurons in order to generate target-specific motor responses. Furthermore, since the lack of motor pool clustering is common in other cranial motor neurons, position-independent connectivity adjustment may be a general principle in brain motor wiring. In fact, resilience to coarse-level positional shifts was previously reported in facial motor neurons in zebrafish[44,45]. Facial motor neurons produce rhythmic operculum movements in a normal frequency even when the entire facial nucleus is shifted anterior to its normal position[44]. In addition, jaw-opening behavior was successfully produced, though with reduced frequency[45]. One key question that remains to be addressed is

whether separate control of different body parts (e.g., operculum and jaw) is achievable when the topographic organization inside the nucleus is missing, which would indicate single-cell-level connectivity specification as we revealed in vagus motor neurons.

**Experience-dependent connectivity refinement**

Topographic organization of cell bodies is similarly coarse or absent in some sensory neurons, including mouse vagus sensory neurons[46,47]; however, specific connectivity is established by topographic sorting of the central axons and synapse-level adjustment. For instance, cell bodies of mouse trigeminal sensory neurons innervating neighboring whiskers are intermingled in the trigeminal ganglion[48]. But their central axons in the brainstem are segregated into two distinct domains called barrelettes, where they synapse on different postsynaptic neurons[37]. While molecular differences play a major role in topographically sorting the central axons of whisker-innervating sensory neurons in prenatal mice, sensory experience from the periphery refines the topographic organization and instructs point-to-point synaptic connections post-natally[49]. Sensory experience gives correlated activity to sensory neurons innervating the same whisker, directing them to converge into the same circuit through the Hebbian mechanism, enabling "neurons that fire together to wire together"[50]. In contrast, sensory neurons innervating different whiskers show less correlated activity and are consequently segregated into different circuits.

It is difficult to imagine how a Hebbian mechanism could generate accurate motor responses however. In many motor neurons, including spinal and vagus motor neurons, axons innervate their peripheral targets early in development and cannot re-target them to match sensory input from the same target in a Hebbian mechanism. Rather, somatodendritic connectivity inside the spinal cord or the brain, when it is established, needs to be so specific that motor neurons innervating common targets fire together for cooperative motor control. This can be accomplished through a developmental positional mechanism if motor neurons innervating the same target are spatially segregated as in monosynaptic spinal circuits as discussed above[22,41]. However, in a continuous topographic map a further, non-Hebbian refinement mechanism is needed.

We provide three lines of evidence that input connectivity of vagus motor neurons is refined in an experience-dependent manner. First, vagus motor neurons are progressively more fine-tuned to designated sensory signals after larval zebrafish start using them. Second, vagus motor neurons that are made ineffective in producing motor outputs by neurotransmission suppression reduce their responsiveness to sensory signals. Third and most importantly, vagus motor neurons increase activity levels when neurotransmission is suppressed from surrounding vagus motor neurons co-innervating the same target. This compensatory change in intact neurons strongly suggests that motor neurons that produce an effective response to upstream signals are "rewarded" by a periphery-to-brain feedback signal that stabilizes input connectivity at the single neuron level. The nature of this signal is unknown. It may be mediated by the retrograde transport of signaling molecules inside motor neurons, such as pMad transcription

factor known to be activated by BMP signaling from the postsynaptic muscles in the *Drosophila* NMJ[51,52]. Alternatively, it could be mediated by sensory feedback, as is used in the vestibulo-occular reflex circuit to globally modify the activity level of eye-rotating motor populations[53]. Though we lack direct evidence, we suspect that single-cell-level adjustment mediated by periohery-to-brain signaling would have a capacity to generate point-to-point synaptic specificity in the intermingled vagus motor population.

We identified that topographically mispositioned neurons extend dendrites into the territory occupied by dendrites of motor neurons innervating the same target, which we termed "adaptive dendritic extensions" and that the formation of adaptive dendritic extensions depends on motor neurons neurotransmission. What could be the mechanism underlying the development of these dendrites? It is plausible that dendritic projections of vagus motor neurons are guided by feedback-mediated synaptic stabilization whereby motor dendrites randomly extend filopodia long distances, and nascent connections that produce relatively effective motor outputs are more stabilized than others. Such a mechanisms was previously proposed based on live imaging of zebrafish tectal neurons[54]. This step could guide the direction of dendritic projections and eventually create dendritic architecture that topographically echoes the already-fixed axonal projection patterns of vagus motor neurons.

**Vagus sensory-motor circuits across vertebrates**

In this study, we investigated input connectivity of vagus motor neurons by analyzing their activity responses to sensory signals. The anatomical correlates of these responses are poorly understood in any system, including in the zebrafish where the direct presynaptic partners of vagus motor neurons are unidentified. Reportedly, many reflexes that involve both sensory and motor components of the vagus are controlled by a 3-neuron circuit (i.e., sensory neuron, interneuron, motor neuron)[3,29,55]. Both in carp and catfish, such simple 3-neuron reflex arcs connect vagus sensory and motor neurons innervating the same pharyngeal locations to generate the oropharyngeal reflex that sorts and expels inedible items from the pharynx[29,55]. It is therefore reasonable to predict that stereotypical pharyngeal reactions against pharyngeal noxious cues in zebrafish larvae are mediated by a similar 3-neuron arc generated from vagus sensory and motor neurons innervating the pharynx. If this is indeed the case, identifying presynaptic neurons of vagus motor neurons would reveal all components of the sensory-motor circuit and allow us to investigate the anatomical basis of specific physiological connectivity. It would be an interesting research direction to determine how single interneurons in the brainstem could identify and bridge functionally appropriate pairs of sensory and motor neurons of the vagus in wiring functional reflex circuits. This question is important because the 3-neuron structure is widely conserved even in mammals for some vagus-mediated reflexes, which include the gastric and pancreatic reflexes[3,56]. It remains poorly explored in any animal how postsynaptic neurons of vagus sensory neurons in the nucleus tractus solitarii (NTS) synapse on specific vagus motor neurons for independent body controls, though remarkable functional topography of NTS neurons was recently reported[57]. The

zebrafish system we established in this study is particularly suitable for addressing this question.

While the simple 3-neuron arc is partly conserved across vertebrates, vagus reflex circuits have meanwhile flexibly modified networks to optimize peripheral body reactions as vertebrates evolved internal body structures and functions. In mouse, pharyngeal muscle activities are reflexively induced by sensory cues in the upper airway for airway protection[58]. Additionally, mammals respond to inflammation-driven noxious signals in the pharynx, not with simple pharyngal muscle contractions, but with the complex cough reflex which is regulated by compound vagus-involved networks in the medulla called the cough center[59]. We hypothesize that acquisition of optimized vagus networks during vertebrate evolution has been accelerated by the plasticity we illustrated in this study, which can modify motor connectivity in the absence of prior genetic adjustment in molecular neuron-neuron recognition.

**ACKNOWLEDGMENTS**
We thank Ajay Dhaka, Koichi Kawakami, and Herwig Baier for transgenic lines. We thank Penny Lam for assisstance with optovin-mediated noxious stimulation in larval zebrafish. We thank the members of the Moens lab for discussion, Jason Stonick for technical help, and Olivia Fitzgerald for zebrafish care. This work was supported by NIH grants R01 (NS109425) and R21 (1R21NS124191) to C.B.M. and the AHA postdoctoral fellowship (19POST34380845) and JSPS overseas research fellowship (202060651) to T.K.

## METHODS AND MATERIALS

### Experimental Model and Subject Details

Zebrafish lines

*Danio rerio* animals were raised at the Fred Hutchinson Cancer Center facility in accordance with institutional animal care and use committee (IACUC)-approved protocols. All experiments were carried out in accordance with IACUC standards. Fish were bred and maintained according to standard protocols. All experimental stages are noted in the figures and text. Sex is not a relevant biological variable in our experiments, which are carried out before sex is determined in zebrafish. Larval zebrafish were fed starting at 5 dpf. Transgenic lines used in this study include: *Tg(isl1:Kaede)*$^{ch103}$ [12] ; *Tg(isl1:Gal4)*$^{fh452}$ [60]; *Tg(isl1:mRFP)*$^{fh1}$ [61] ; *Tg(isl1:EGFPCAAX)*$^{fh474}$ [12]; *Tg(p2rx3b:GFP)*$^{sl1}$ [62] *TgBAC(chata:GAL4-VP16)*$^{mpn202}$ [63]; *Tg(UAS-E1B:Kaede)*$^{s1999t}$ [64]; Tg(*UAS:GCaMP6s*$^{13A}$) [65], *UAS:BoTxBLC-GFP*$^{icm21}$ [35], *HuC:H2B-GCaMP6s* [66]. Lines generated for this study include *Tg(isl1:H2B-GCaMP6s), Tg(UAS:hoxb5a-p2a-GFPcaax)fh567, Tg(UAS:DN-RAR-p2a-GFP-CAAX)*$^{fh575}$, *Tcf21*$^{Gal4(fh557)}$, *Trpa1b*$^{Gal4(fh577)}$.

### Method Details

Generation of transgenic lines

50 pg of the Tol2 plasmid, *UAS:hoxb5a-p2a-GFP-CAAX or UAS:DN-RAR-p2a-GFP-CAAX,* which was generated previously[11,12], was injected into *Tg(isl1:Gal4)* embryos at the one-cell stage together with 50 pg of Tol2 transposase mRNA. The Tol2 plasmid *isl1:H2B-GCaMP6s* was generated in this study. The *H2B-GCaMP6s* sequence was obtained from the Addgene plasmid *Tol2-elav3-H2B-GCaMP6s* (#59530), and the *isl1* CREST1 enhancer is from[31]. 50 pg of the Tol2 plasmid *isl1:H2B-GCaMP6s* was injected into wild type embryos at the one-cell stage together with 50 pg of Tol2 transposase mRNA. Injected embryos were screened for GFP-CAAX or GCaMP6s expression and grown to adulthood. Stable lines were then identified in the F1 generation.

*Tcf21*$^{Gal4}$, *Trpa1b*$^{Gal4}$, were generated using the CRISPR/Cas9-mediated knock-in strategy outlined in[67]. The donor plasmids GBait-hs-Gal4 was provided by the Higashijima lab.

Kaede photoconversion

Kaede photoconversion to visualize target groups of vagus motor neurons was described previously [11,12]. In brief, larvae were anesthetized with 200 mg/l 3-aminobenzoic acid ethyl ester (MS-222) (Sigma-Aldrich, A5040), embedded laterally in 1.2% low-melting-point (LMP) agarose (Invitrogen, 16520), and imaged live on a Zeiss LSM 700 inverted confocal microscope. A region of interest (ROI), which was drawn over an individual branch, was photoconverted by 100 iterations of 405 nm laser at 8% power. Kaede$^{Red}$ signals in the vagus motor nucleus was imaged at least 1 hr after the photoconversion.

For sequential photoconversion in Fig 1C and FigS1, the cycle of photoconversion and image acquisition was repeated for different branches in the same animal, with at least 1 hr between

each photoconversion and imaging. To determine Kaede$^{Red}$ signals generated by the latest photoconversion but not by the prior photoconversions, one preceding Kaede$^{Red}$ image was subtracted from the latest Kaede$^{red}$ image. To subtract an image, the Image Calculator function of Fiji was used after Kaede$^{Red}$ images from different time points were aligned by Descriptor-based registration function of Fiji.

Calcium imaging

Calcium imaging was done on Zeiss LSM700 confocal microscope with single z-plain acquisition at 4 Hz. For focal noxious stimulation, larval zebrafish were incubated with 10 µM optovin dissolved in 0.2% DMSO for at least 2 hours prior to calcium imaging. Larvae were then embedded laterally in 1.2% LMP agarose without tricaine treatment. To focally activate optovin, 405 nm confocal laser at 6% power was given for ~2 seconds to a region of interest drawn over the anterior pharynx, posterior pharynx, or the esophagus. Photostimulation was repeated within the same animal at 25-40 second intervals (100 frames for nucleus imaging and 150 frames for axonal imaging). For AITC-mediated noxious stimulation, 10 mM AITC dissolved in 1% DMSO was bath applied onto agarose-mounted animals during calcium imaging.

To provide mechanosensory stimulation to the larval esophagus, a glass needle pulled from a Wiretrol 10 µl capillary micropipette (Drummond Scientific, 21-175B) was filled with mineral oil (Sigma) and inserted into the esophagus through the stomach, in laterally agarose-embedded larval zebrafish without tricaine treatment while on the confocal microscope stage. During calcium imaging from the motor nucleus, drops of mineral oil (~ø 30 µm) were delivered inside the esophagus every 25 seconds (every 100 frames). To identify the viscera-targeting neurons in animals that carry *Tg(isl1:Kaede)*, Kaede was photoconverted in the visceral branch, and Kaede$^{Red}$ was imaged at least 1 hour after the photoconversion. All remaining Kaede$^{Green}$ signals were photoconverted to Kaede$^{Red}$ prior to GCaMP imaging.

Vagus neuron transplantation

Transplantation was performed as described previously[12,28] on 2 dpf embryos in Fig. 4 and 1 dpf embryos for Fig. 6g-j. Donor embryos carrying Tg(*isl1:mRFP*) and Tg(*isl1:H2B-GCaMP6s*) (nuclear GCaMP6s) were used in Fig. 4e-o and Fig. 6g-j for nuclear GCaMP imaging, whereas donor embryos carrying Tg(*isl1:mRFP*), Tg(*chata:Gal4*) and Tg(*UAS:GCaMP6s*) (cytoplasmic GCaMP6s) were used in Fig4. a-d for axonal GCaMP imaging. Host embryos carrying Tg(isl1:Gal4, UAS-BoTxBLC-GFP) were used in Fig. 4e-o and Fig. 6g-j, whereas Tg(chata:Gal4, UAS-BoTxBLC) was used in Fig 4. a-d. chata:Gal4 was selected because isl1:Gal4-driven GFP expression in the heart overlaps with the GCaMP signals in motor axons. For transplantation, Donor and host embryos were both anesthetized with 200 mg/l MS-222 and laterally embedded in 1.2 % LMP agarose. A glass needle pulled from a Wiretrol 10 µl capillary micropipette (Drummond Scientific, 21-175B) was inserted from the dorsal side into the hindbrain at a 45° angle to the body axis at the level of the vagus nucleus. RFP-expressing vagus neurons were collected from the particular topographic position of the donor nucleus stated in the text. The needle was then similarly inserted into the vagus nucleus of host embryos, and ~10 RFP-neurons were placed into a designated position of the host nucleus. Following transplantation, larvae were unmounted from agarose and placed into normal Ringer's solution+1% Pen Strep (Gibco, 15140-122) until

imaging at 10-11 dpf. Because a majority of neurons transplanted after 40 hpf disappeared by 10 dpf or showed no calcium transients at all, neurons that showed at least one calcium transient were used for quantification.

Mosaic transgenic labeling for dendritic imaging

Sparse transgenic labeling of vagus motor neurons was carried out as described previously[12]. In brief, one-cell-stage Tg(isl1:Gal4) embryos were injected with 50 pg of *Tol2* mRNA, combined with 25 pg of UAS:GFP-CAAX plasmid [12] . Injected animals were screened for sparse GFP expression at 3 dpf and raised to 7-8 dpf for confocal imaging.

**Quantification and Statistical Analysis**

Quantification of calcium responses in the motor nucleus

Calcium imaging data of the vagus motor nucleus were first motion-corrected by CaImAn[68], followed by cellular segmentation by the machine-learning-based method Cellpose[69]. Significant calcium transients in individual regions of interest (ROIs) were then detected by the MatLab-based toolbox developed previously[70] where (1) the noise in the fluorescent signal was estimated from the standard deviation of the baseline fluorescent variations and (2) *Dynamic Threshold Method* was used to estimate the significant fluorescent transients. ROIs are counted as responders in Fig 3c,i and 6b, when they show significant calcium transients at least 4 times following noxious stimulation to the same body spot repeated 5 times. To visualize significant dF/F0 transients in Fig 3b,h, and Fig 6c, all dF/F0 values except significant ones were set to 0 and significant dF/F0 transients over 6 were set to 6. For pair-wise correlation analysis in Fig. 3f, averaged dF/F0 values from the 20 frames following noxious stimulation were plotted for all ROIs collected from 7 larvae. Correlation coefficient (R) was measured to determine the level of correlation. Because ROIs for hoxb5a-positive neurons contain GFP-CAAX-derived green fluorescent signals, to compare changes in GCaMP fluorescence in GFP-CAAX-positive (hoxb5a-positive) neurons and GFP-CAAX-negative neighbors (Fig.7g), dF/F0 values are normalized into the Z-score. Temporal correlation in significant transients was analyzed for correlation coefficient between a single ROI and all other ROIs (vagus motor neurons in the same imaging plane), which was color coded in Fig. 7g. The correlation coefficient that single anterior neurons (either ectopic or not) show with all other anterior neurons (0~45 µm, where pharynx-targeting neurons reside) and posterior neurons (75 µm~) were each averaged for $Corr^{Ant}$ and $Corr^{Post}$, respectively. Correlation index in Fig 7h was calculated as $Corr^{Ant}/(Corr^{Ant}+Corr^{Post})$, where Wilcoxon matched-pairs singled rank test was used. Significant correlation level was determined as described previously [71].

Quantification of calcium responses in pharyngeal arches

GCaMP signals were measured from ROIs drawn manually over the pharyngeal arches PA4, 5, 6. Averaged dF/F0 values from the 10 frames following noxious stimulation were plotted in Fig 2d, g, j, where paired t-test was used. Response tuning index was calculated for individual ROIs as $(dF^A/F0) / [(dF^A/F0)+ (dF^P/F0)]$, where $dF^A/F0$ and $dF^P/F0$ indicate averaged dF/F0 following noxious stimulation to anterior and posterior pharynx, respectively. Paired nonparametric test (Wilcoxon matched-pairs signed rank test) was used.

Quantification of calcium responses in vagus sensory axons

To compare the axonal activity in vagus sensory neurons elicited by optovin stimulation to different body locations, cumulative density distribution of dF/F0 was measured. To calculate dF/F0 for each pixel, the 20 frames prior to noxious stimulation were averaged into a projection image, “pre-image”, and the 20 frames after stimulation were similarly averaged into a projection image, “post-image”. Image Calculator function of Fiji was used to subtract the pre-image from the post-image for dF, which was then divided by the pre-image, generating a 2D image with dF/F0 in each pixel. Cumulative density distribution was then quantified for the anterior-posterior extent of the axon terminals as described previously[28]. The half-maximum value of the cumulative density distribution was plotted in Fig. S2i and statistically analyzed by t-test.

## Figure Legends

**Figure 1. Vagus motor neurons targeting different peripheral branches are intermingled in the brain.**
**(a)** 3 day post-fertilization (dpf) larva with cranial motor neurons in magenta and cranial sensory neurons in green. Vagus motor neurons (indicated by mXn) innervate the pharyngeal arches (PA4-7) and the viscera (v). Sensory neurons that project in the vagus nerve lie in epibranchial ganglia (EB2-4) associated with PA4-6 respectively, and in the large nodose ganglion (N). **(b)** Schematic of vagus motor neuron topography. Vagus motor neurons that target different branches are shown in different colors. Reproduced from Isabella AJ et al. 2020 [11]. **(c)** Vagus motor neuron target groups in a single 4 dpf larva visualized by sequential retrograde lebeling and imaging. Each target group is shown a different color, with corresponding colored lines indicating the anterior-posterior (A-P) extent of each motor neuron territory. **(d-h)** Retrograde labeling of individual target groups in 4 dpf larvae showing dendritic field overlap. Lines indicate the A-P extent of the individual target group dendrites (magenta) and the entire vagus motor dendritic field (green). For overlap quantitation see Fig. S1. Scale bar: 50 µm.

**Figure 2. Focal noxious stimulation to the pharynx elicits motor responses that become more specific over time. (a)** 4 dpf fish showing motor neurons (magenta) and cranial muscles (green). The PA4, PA5, and PA6 branches innervate structurally equivalent muscles while the PA7 branch innervates a different muscle (arrowhead). **(a')** Schematic showing the anterior (A) and posterior (P) pharyngeal spots illuminated by UV laser for optovin activation. The rectangle shows the calcium imaging area. **(b-l)** Calcium imaging of pharyngeal muscles **(a-e)** and of vagus motor axons **(f-l)**. **(b)** GCaMP6s activity in pharyngeal muscles in response to A (top) and P (bottom) stimulation at 10 dpf. The regions of interest (ROIs) used for quantification are indicated by orange circles **(c)** averaged calcium traces for pharyngeal muscle responses from 10 animals over 4 iterations of alternating A and P stimulation. **(d)** Comparison of calcium responses between PA4, PA5 and PA6 muscles in the absence and presence of optovin at 10 dpf. n=10 larvae for each condition. **(e)** Tuning of the response to focal stimulation at 10 dpf (see text for explanation of the "response tuning index"). **(f, i)** Vagus motor branches innervating PA4-6 were analyzed at 11 dpf **(f)** and 4 dpf **(i)** through calcium imaging in response to A (left) and P (right) noxious stimulation. **(g, j)** Averaged calcium traces of motor branch responses over 4 iterations of alternating A and P stimulation at 11 dpf (**g**, n=11) and 4 dpf (**j**, n=10). **(h, k)** Comparison of calcium responses between PA4, PA5 and PA6 branches at 11 dpf (**h,** n=11) and 4 dpf (**k**, n=10). **(l)** Response tuning index for 4 dpf (n=10), 7 dpf (n=11), and 11 dpf (n=11). Scale bar 50 µm. Statistics in panels **d**, **h** and **k**: paired t-test. Statistics in panels **e**, **l**: Wilcoxon matched-pairs singled rank test. ** indicates $p<0.01$, * indicates $0.01<p<0.05$, N.S. indicates $0.05<p$ throughout the paper.

**Figure 3. Focal noxious stimulation elicits responses in spatially overlapping motor neurons.** Calcium responses in vagus motor neurons in response to focal noxious stimulation at 10 dpf **(a-f)** and 4 dpf **(g-k)**. **(a, g)** Vagus motor neurons that repeatedly exceed a threshold response to repeated focal stimulations to anterior pharynx (top), posterior pharynx (middle) and

esophagus (bottom) in representative 10 dpf **(a)** and 4 dpf **(g)** larvae. **(b,h)** Calcium traces for the neurons in the larvae in **(a, g)**, respectively, in response to five cycles of anterior pharynx (A), posterior pharynx (P) and esophagus (E) noxious stimulation. Neurons aligned from top to bottom corresponding to their anterior-to-posterior position in the nucleus. The magnitude of GCaMP signals is coded in the heat-color. **b'**: responses to focal UV illumination in the absence of optovin. Spontaneous firing (arrowhead) was observed independent of illumination timing**.** **(c, i)** The percentage of GCaMP6s-expressing neurons in each of ten 15-µm bins along the A-P axis of the vagus motor nucleus that repeatedly respond to repeated A (left) and P (right) pharyngeal stimulation at 10 dpf (**c**, n=7 larvae) and 4 dpf (**i**, n=7 larvae). **(c')** responses in the absence of optovin (n=7 larvae). **(d, j)** The detailed position within the first 45 µm of the motor nucleus of the responding (+) and non-responding (-) neurons in **c, i** for A and P stimulation at 10 dpf **(d)** and 4 dpf **(j)**. **(e, k)** The response tuning index for all motor neurons that repeatedly respond to A or P or both stimulation at 10 dpf (**e**, n=84 neurons in 7 animals) and 4 dpf (**k**, 218 neurons in 7 fish). **(f)** Correlation analysis of responses of motor neurons to stimuli in the same and different locations[57]. Left: Dots represent all analyzed neurons collected from 7 animals, which are plotted based on the GCaMP levels (dF/F0) following two noxious stimulations at the same (top graphs) or different (bottom graphs) locations. Correlation coefficient (R) is measured as the indication of correlation levels. Right: Correlation matrix for all 15 stimulation events, with the level of correlation (R) color coded. The boxes outlined in white are shown in the graphs on the left. Scale bar in **a, g**=50 µm.

**Figure 4. Spatially appropriate responses of vagus motor neurons can be established independent of their position in the topographic map.**

**(a)** Top: transplantation approach for manipulating the topographic organization of pharynx-targeting neurons. Bottom: at 10 dpf, after axons of transplanted neurons have reinnervated their original targets, focal noxious stimulation is delivered as described above to the anterior (A) or posterior (P) pharynx, and GCaMP6s responses in the axons of donor-derived neurons are recorded. **(b)** Donor-derived neurons that locate at the same A-P position (magenta) regenerate axons that re-innervate the pharyngeal arches (arrowheads in **b'**). **(c)** Averaged GCaMP6s traces of donor-derived axons in response to alternating A and P stimuli in larva shown in **b**. Signals are weaker than in intact animals because of the smaller number of GCaMP6s-expressing axons. **(d)** Response Tuning Index for n=14 transplanted animals (right) and n=6 untransplanted control animals (left) in which all vagus motor neurons express GCaMP with Tg(chata:Gal4, UAS:GCaMP6s). **(e, i)** Transplantation approaches for generating positionally incorrect motor neurons. Anterior **(e)** or posterior **(i)** vagus motor neurons are transplanted to the middle region of the nucleus (40-60% of its length, a position normally occupied by PA7-innervating neurons). At 10 dpf, after axons have regrown to their original targets, GCaMP6s responses of transplanted neurons to focal noxious stimulation are measured. **(f)** GCaMP response of mispositioned anterior neuron to pharynx stimulation. **(g, h)** The axons **(g)** and dendrites **(h)** of transplanted anterior-derived vagus motor neurons in the same larval fish. **(j)** GCaMP6s response of mispositioned posterior neurons to pharynx stimulation. **(k, l)** Absence of axons in

the pharyngeal arches **(k)** and posterior polarization of dendrites **(l)** of mispositioned posterior neurons in the same larval fish. **(m)** Average Calcium responses following noxious stimulation to A, P or esophagus (E) is shown for 6 ectopic anterior-projecting (left) and 6 ectopic posterior-projecting (right) neurons positioned in the middle of the motor nucleus. **(n)** the highest dF/F0 value from A and P stimulation for each neuron in (**m**). **(o)** The proportion of the area of dendrites anterior to the nucleus as a fraction of the total dendritic area. 5 animals were used for both conditions. Statistics in **d**: Wilcoxon matched-pairs singled rank test. Statistics in **m,o**: t-test. Scale bars 50 µm.

**Figure 5. Ectopic vagus motor neurons form adaptive dendritic projections dependent on motor neurotransmission.**
**(a-d)** sparse expression of GFP-CAAX **(a,b; m** or DN-RAR-p2A-GFP-CAAX **(c-f; green)** in one or a few vagus motor neurons in the anterior **(a)** or posterior **(b-d)** part of the vagus motor nucleus at 7-8 dpf. Green lines indicate the A-P extent of the labeled neuron's dendrites, and magenta brackets indicate the length of the entire vagus motor dendritic territory. Arrowheads in c' and d' indicate the anterior targeted dendrites of posterior neurons. (**e, f)**: sparse expression of DN-RAR-p2A-GFP-CAAX in a posterior vagus motor neuron (arrowheads, green membrane) in larvae expressing BoTXBLC-GFP throughout the vagus motor nucleus (cytoplasmic green). **(g)** Comparison of dendritic architecture of posterior neurons under the conditions indicated in 7-8 dpf larvae. Posterior motor neurons whose dendrites extend beyond the posterior 40% of the dendritic neuropil were defined as "neurons with anterior dendritic projections". The number in the bar graph indicates the sample number used in the analysis. Statistics: Chi-Square test; scale bar: 50 µm.

**Figure 6. Activity of pharynx-targeting motor neurons depends on effective neurotransmission.**
**(a-d)** BoTx-BLC expression in motor neurons reduces the number of vagus motor neurons responding to pharyngeal noxious stimulation. **(a)** BoTx-BLC-expressing vagus motor neurons that repeatedly exceed the same threshold response as in Fig. 3a,h to repeated focal stimulations to anterior pharynx (A, top), posterior pharynx (P, middle) and esophagus (E, bottom) in a representative 10 dpf larva. **(b)** The percentage of BoTx-BLC-expressing motor neurons in each of ten 15 µm bins along the A-P length of the motor nucleus that repeatedly respond to anterior (left), posterior (middle) and AITC stimulation (right) at 10 dpf (n=7 larvae). **(c)** Calcium traces for all imaged neurons from the larva in **(a)** over four cycles of A, P, and E stimulation**.** Neurons are aligned from top to bottom corresponding to their anterior-to-posterior position in the nucleus. The level of GCaMP signals is coded in the heat map. AITC was applied in the same animal following focal stimulations. **(d)** Comparison of the number of responding neurons in the anterior-most 45 µm of the motor nucleus between control (from Fig. 3c) and BoTx-expressing animals (n=7 larvae per condition). **(e,e')** Photoconversion of PA6-innervating vagus motor neurons in control **(e)** and BoTX-BLC-expressing **(e')** larvae at 4dpf. Left panels show unconverted (green) and photoconverted (magenta) neurons while the right

panels show only photoconverted neurons and their dendrites. Lines indicate the A-P extent of the photoconverted dendrites (magenta) and the entire vagus motor dendritic field (green). **(f)** The A-P extent (in µm) of the dendrites of PA6-innervating motor neurons in **e**. **(g)** Schematic of the transplantation approach for generating BoTx-negative neurons in a BoTx-expressing host vagus motor nucleus. **(h)** Donor-derived neurons (magenta, arrowheads) in a BoTx-expressing host motor nucleus (blue) before (left) and after (right) posterior pharynx stimulation. GCaMP signal (green) in donor-derived neurons (red) creates a white pseudocolor. **(i)** Pharyngeal arches of a host larva innervated by donor-derived axons (magenta). **(j)** Calcium response to A, P and E focal stimulation at 10 dpf of non-BoTx-expressing neurons transplanted into a non-BoTX-expressing (left, n=11) or to a BoTx-expressing (right, n=11) host motor nucleus. Statistics in **d** and **j**: t-test. scale bar: 50 µm.

**Figure 7. Viscera-innervating neurons integrate into a visceral circuit independent of their position in the motor nucleus.**

**(a)** Schematic of esophagus stretch method for generating a specific response in posterior vagus motor neurons **(b)** Example of a posterior-restricted GCaMP6s response following oil injection into the esophagus. Arrowheads show examples of vagus motor neurons with calcium imcreases. **(c)** Schematic of approach for generating ectopic viscera-innervating neurons by sparse expression of *hoxb5a*-GFP (green). Ectopic neurons innervating the viscera (magenta) are identified by photoconversion of the visceral branch. All neurons express H2B-GCaMP6s. **(d, e)** Example of GCaMP imaging of ectopic viscera-innervating motor neurons. **(d)** step 1. Viscera-innervating anterior motor neurons #1 and #2 (magenta outlined arrowheads) are identified by photoconversion of the visceral branch. **(e) top**: step2. After photoconverting the whole motor nucleus (now magenta), membrane GFP identifies *hoxb5a*-expressing motor neurons (green filled arrowheads). Not all *hoxb5a*-expressing neurons extend in the visceral branch (green arrowhead without magenta outline). **Bottom**: step3. GCaMP imaging after esophagus stretch. Anterior viscera-innervating neuron #1 responds while neuron #2 does not. **(f, f')** computational analysis of correlation between ectopic viscera-innervating motor neurons (#1 **(f)** or #2 **(f')**) and all other neurons in the same focal plane. All the time frames acquired from calcium imaging were used for the correlation analysis. Heat map ranges from anti-correlated (blue) to fully correlated (red). White dotted circles indicate neurons below the significant correlation level. **(g)** normalized dF/F0 (z-score) was quantified at the single neuron level. Larvae with viscera-targeting neurons in the anterior region (~45 µm) in which oil injection caused responses in the posterior region were used in the analysis, n=10 ectopic neurons from 8 larvae at 7 dpf. On the left side of the graph, the z-score of individual ectopic motor neurons is shown compared to the average of this value from all immediate neighboring neurons (within 8 µm). Five ectopic neurons that showed high calcium responses were categorized as responders (red, including neuron #1 shown in **f**) and the others as non-responders (blue; including neuron #2 shown in **f'**). On the right side of the graph, the z-score values averaged for all neurons in the same 15µm bin (excluding hoxb5a-positive neurons) in the same larvae are shown. **(h)** Correlation index (see Methods) was quantified for 10 ectopic neurons and their immediate neighbors analyzed

in **g**. Colors indicate two groups of ectopic neurons defined in **g**, while the statistical comparison was done altogether (without separating to the two groups). Statistics in **g**, **h**: paired nonparametric t-test (Wilcoxon matched-pairs signed rank test).

**Figure S1 (for Figure 1). The dendrites of pharynx-targeting motor neurons are significantly overlapping.**
**(a)** Schematic of approach: Sequential photoconversion for the two pharyngeal branches, PA4 and PA6, in 4 dpf larvae expressing Tg(isl1:Kaede). Imaging is done after each photoconversion, so the dendritic territory measured after the second photoconversion includes dendrites of both target groups (PA4+PA6 in this example). The square indicates the area used for quantification in **b**. **(b)** quantification of dendritic overlap between vagus target groups. The top bar shows the ratio of the PA4 dendritic area to the PA4+PA6 dendritic area, determined by sequential PA4>PA6 photoconversion. The second bar is the converse ratio, determined by sequential PA6>PA4 photoconversion. If there were no overlap between PA4 and PA6 dendritic territories, PA6/PA4+PA6 would be predicted to be equal to 1-PA4/PA4+PA6. In fact, PA6/PA4+PA6 (avg.=0.9, n=4) > 1-PA4/PA4+PA6 (avg 0.35, n=4), leading us to reject the null hypothesis that there is no dendritic overlap. In contrast, sequential photoconversion demonstrates no overlap between the dendritic fields of PA6 and viscera-innervating target groups (lower two bars). The level of dendritic overlap indicated from this analysis is schematized below the graph. **(c-f)** The overlay of the image after the first photoconversion (magenta) and that after the second photoconversion (green). The overlay shows the target group photoconverted first in white (i.e., magenta + green). The order of sequential photoconversion is indicated at the left. 4 dpf larvae expressing Tg(isl1:kaede) were used. Statistics in b: t-test. Scale bar 50 µm.

**Figure S2 (for Figure 2). Vagus sensory neurons that express Trpa1b respond to optovin stimulation.**
**(a)** Trpa1b-expressing vagus sensory neurons (green) in 7 dpf larva. Squares indicate the areas shown in b, g (orange) and d (blue). Epi: epibranchial ganglia. **(a')** Overlay with vagus motor neurons (magenta). mXn: vagus motor neuron **(b)** Anterograde labeling by Kaede photoconversion of the central processes of Trpa1b-expressing sensory neurons innervating pharyngeal arches PA4, 5, or 6. **(c)** Quantification of overlap between central processes of PA4 and PA6-innervating sensory neurons, as in Fig. S1b. **(d)** GCaMP signals in sensory neuron cell bodies at 7 dpf following anterior and posterior pharyngeal stimulation. The magnitude of GCaMP signals is coded in the heat-color. The purple boxes indicate the region of violet light illumination to activate optovin. Arrowhead indicate neurons responding to optovin activation. **(e)** Calcium traces of larva shown in d. Neurons are aligned from top-to-bottom corresponding to anterior-to-posterior positioning in the periphery. Noxious stimulation to the anterior (A) and posterior (P) pharynx was each repeated five times. **(f)** Correlation coefficient between activity patterns following two stimulations as in Fig. 2f. Dots represent all neurons analyzed. n= 317 neurons in 7 animals (7 dpf). **(f')** Correlation matrix for all 10 stimulation events, with the level of correlation (R) color coded. **(g-i)** The axonal responses of vagus sensory neurons to focal

optovin stimulation are topographically organized throughout multiple stages. **(g)** Calcium signals following optovin stimulations are shown in the color of heat. **(h)** The anterior-posterior organization of axonal activities is quantified as cumulative density distribution of dF/F0 (see Method) following anterior pharynx (A), posterior pharynx (P) and esophagus (E) stimulation. The A-P extent of the axon terminals is converted into the scale of 0 (anterior most) to 100 (posterior most). n=7 from 7 dpf larvae. Dotted lines show results from individual animals, with the thick line indicating the average. **(i)** cumulative density midpoints of dF/F0 from 4 dpf (n=7), 7 dpf (n=7), and 10 dpf (n=6) are shown. Statistics in c: t-test, and statistics in i: paired t-test. Scale bars: 50 µm.

**REFERENCES**


1 Prescott, S. L. & Liberles, S. D. Internal senses of the vagus nerve. *Neuron* **110**, 579-599, doi:10.1016/j.neuron.2021.12.020 (2022).

2 Neuhuber, W. L. & Berthoud, H. R. Functional anatomy of the vagus system - Emphasis on the somato-visceral interface. *Auton Neurosci* **236**, 102887, doi:10.1016/j.autneu.2021.102887 (2021).

3 Mussa, B. M. & Verberne, A. J. The dorsal motor nucleus of the vagus and regulation of pancreatic secretory function. *Exp Physiol* **98**, 25-37, doi:10.1113/expphysiol.2012.066472 (2013).

4 Coverdell, T. C., Abbott, S. B. G. & Campbell, J. N. Molecular cell types as functional units of the efferent vagus nerve. *Semin Cell Dev Biol*, doi:10.1016/j.semcdb.2023.07.007 (2023).

5 Yuan, H. & Silberstein, S. D. Vagus Nerve and Vagus Nerve Stimulation, a Comprehensive Review: Part I. *Headache* **56**, 71-78, doi:10.1111/head.12647 (2016).

6 Isabella, A. J. & Moens, C. B. Development and regeneration of the vagus nerve. *Semin Cell Dev Biol*, doi:10.1016/j.semcdb.2023.07.008 (2023).

7 Bieger, D. & Hopkins, D. A. Viscerotopic representation of the upper alimentary tract in the medulla oblongata in the rat: the nucleus ambiguus. *J Comp Neurol* **262**, 546-562, doi:10.1002/cne.902620408 (1987).

8 Norgren, R. & Smith, G. P. Central distribution of subdiaphragmatic vagal branches in the rat. *J Comp Neurol* **273**, 207-223, doi:10.1002/cne.902730206 (1988).

9 Fox, E. A. & Powley, T. L. Longitudinal columnar organization within the dorsal motor nucleus represents separate branches of the abdominal vagus. *Brain Res* **341**, 269-282, doi:10.1016/0006-8993(85)91066-2 (1985).

10 Tao, J. *et al.* Highly selective brain-to-gut communication via genetically defined vagus neurons. *Neuron* **109**, 2106-2115 e2104, doi:10.1016/j.neuron.2021.05.004 (2021).

11 Isabella, A. J., Barsh, G. R., Stonick, J. A., Dubrulle, J. & Moens, C. B. Retinoic Acid Organizes the Zebrafish Vagus Motor Topographic Map via Spatiotemporal Coordination of Hgf/Met Signaling. *Dev Cell* **53**, 344-357 e345, doi:10.1016/j.devcel.2020.03.017 (2020).

12 Barsh, G. R., Isabella, A. J. & Moens, C. B. Vagus Motor Neuron Topographic Map Determined by Parallel Mechanisms of hox5 Expression and Time of Axon Initiation. *Curr Biol* **27**, 3812-3825 e3813, doi:10.1016/j.cub.2017.11.022 (2017).

13 Kitamura, S., Ogata, K., Nishiguchi, T., Nagase, Y. & Shigenaga, Y. Location of the motoneurons supplying the rabbit pharyngeal constrictor muscles and the peripheral course of their axons: a study using the retrograde HRP or fluorescent labeling technique. *Anat Rec* **229**, 399-406, doi:10.1002/ar.1092290312 (1991).

14 Veerakumar, A., Yung, A. R., Liu, Y. & Krasnow, M. A. Molecularly defined circuits for cardiovascular and cardiopulmonary control. *Nature* **606**, 739-746, doi:10.1038/s41586-022-04760-8 (2022).

15 Dasen, J. S. Establishing the Molecular and Functional Diversity of Spinal Motoneurons. *Adv Neurobiol* **28**, 3-44, doi:10.1007/978-3-031-07167-6_1 (2022).

16 Shin, M. M., Catela, C. & Dasen, J. Intrinsic control of neuronal diversity and synaptic specificity in a proprioceptive circuit. *Elife* **9**, doi:10.7554/eLife.56374 (2020).
17 Baek, M., Pivetta, C., Liu, J. P., Arber, S. & Dasen, J. S. Columnar-Intrinsic Cues Shape Premotor Input Specificity in Locomotor Circuits. *Cell Rep* **21**, 867-877, doi:10.1016/j.celrep.2017.10.004 (2017).
18 Levine, A. J., Lewallen, K. A. & Pfaff, S. L. Spatial organization of cortical and spinal neurons controlling motor behavior. *Curr Opin Neurobiol* **22**, 812-821, doi:10.1016/j.conb.2012.07.002 (2012).
19 Balaskas, N., Ng, D. & Zampieri, N. The Positional Logic of Sensory-Motor Reflex Circuit Assembly. *Neuroscience* **450**, 142-150, doi:10.1016/j.neuroscience.2020.04.038 (2020).
20 Balaskas, N., Abbott, L. F., Jessell, T. M. & Ng, D. Positional Strategies for Connection Specificity and Synaptic Organization in Spinal Sensory-Motor Circuits. *Neuron* **102**, 1143-1156 e1144, doi:10.1016/j.neuron.2019.04.008 (2019).
21 Jessell, T. M., Surmeli, G. & Kelly, J. S. Motor neurons and the sense of place. *Neuron* **72**, 419-424, doi:10.1016/j.neuron.2011.10.021 (2011).
22 Surmeli, G., Akay, T., Ippolito, G. C., Tucker, P. W. & Jessell, T. M. Patterns of spinal sensory-motor connectivity prescribed by a dorsoventral positional template. *Cell* **147**, 653-665, doi:10.1016/j.cell.2011.10.012 (2011).
23 Kirshner, H. S. Causes of neurogenic dysphagia. *Dysphagia* **3**, 184-188, doi:10.1007/BF02407221 (1989).
24 Santoso, L. F., Kim, D. Y. & Paydarfar, D. Sensory dysphagia: A case series and proposed classification of an under recognized swallowing disorder. *Head Neck* **41**, E71-E78, doi:10.1002/hed.25588 (2019).
25 Cunningham, E. T., Jr., Ravich, W. J., Jones, B. & Donner, M. W. Vagal reflexes referred from the upper aerodigestive tract: an infrequently recognized cause of common cardiorespiratory responses. *Ann Intern Med* **116**, 575-582, doi:10.7326/0003-4819-116-7-575 (1992).
26 Cutsforth-Gregory, J. K. & Benarroch, E. E. Nucleus of the solitary tract, medullary reflexes, and clinical implications. *Neurology* **88**, 1187-1196, doi:10.1212/WNL.0000000000003751 (2017).
27 Herbst, J. J., Minton, S. D. & Book, L. S. Gastroesophageal reflux causing respiratory distress and apnea in newborn infants. *J Pediatr* **95**, 763-768, doi:10.1016/s0022-3476(79)80733-7 (1979).
28 Isabella, A. J., Stonick, J. A., Dubrulle, J. & Moens, C. B. Intrinsic positional memory guides target-specific axon regeneration in the zebrafish vagus nerve. *Development* **148**, doi:10.1242/dev.199706 (2021).
29 Finger, T. E. Evolution of gustatory reflex systems in the brainstems of fishes. *Integr Zool* **4**, 53-63, doi:10.1111/j.1749-4877.2008.00135.x (2009).
30 Ikenaga, T., Ogura, T. & Finger, T. E. Vagal gustatory reflex circuits for intraoral food sorting behavior in the goldfish: cellular organization and neurotransmitters. *J Comp Neurol* **516**, 213-225, doi:10.1002/cne.22097 (2009).
31 Higashijima, S., Hotta, Y. & Okamoto, H. Visualization of cranial motor neurons in live transgenic zebrafish expressing green fluorescent protein under the control of the islet-

1 promoter/enhancer. *J Neurosci* **20**, 206-218, doi:10.1523/JNEUROSCI.20-01-00206.2000 (2000).
32 Altschuler, S. M., Bao, X. M. & Miselis, R. R. Dendritic architecture of nucleus ambiguus motoneurons projecting to the upper alimentary tract in the rat. *J Comp Neurol* **309**, 402-414, doi:10.1002/cne.903090309 (1991).
33 Kokel, D. *et al.* Photochemical activation of TRPA1 channels in neurons and animals. *Nat Chem Biol* **9**, 257-263, doi:10.1038/nchembio.1183 (2013).
34 Lee, G. H., Chang, M. Y., Hsu, C. H. & Chen, Y. H. Essential roles of basic helix-loop-helix transcription factors, Capsulin and Musculin, during craniofacial myogenesis of zebrafish. *Cell Mol Life Sci* **68**, 4065-4078, doi:10.1007/s00018-011-0637-2 (2011).
35 Sternberg, J. R. *et al.* Optimization of a Neurotoxin to Investigate the Contribution of Excitatory Interneurons to Speed Modulation In Vivo. *Curr Biol* **26**, 2319-2328, doi:10.1016/j.cub.2016.06.037 (2016).
36 Cline, H. T., Lau, M. & Hiramoto, M. Activity-dependent Organization of Topographic Neural Circuits. *Neuroscience* **508**, 3-18, doi:10.1016/j.neuroscience.2022.11.032 (2023).
37 Kitazawa, T. & Rijli, F. M. Barrelette map formation in the prenatal mouse brainstem. *Curr Opin Neurobiol* **53**, 210-219, doi:10.1016/j.conb.2018.09.008 (2018).
38 Zou, D. J. *et al.* Postnatal refinement of peripheral olfactory projections. *Science* **304**, 1976-1979, doi:10.1126/science.1093468 (2004).
39 Sigrist, S. J., Reiff, D. F., Thiel, P. R., Steinert, J. R. & Schuster, C. M. Experience-dependent strengthening of Drosophila neuromuscular junctions. *J Neurosci* **23**, 6546-6556, doi:10.1523/JNEUROSCI.23-16-06546.2003 (2003).
40 Nikaki, K., Sawada, A., Ustaoglu, A. & Sifrim, D. Neuronal Control of Esophageal Peristalsis and Its Role in Esophageal Disease. *Curr Gastroenterol Rep* **21**, 59, doi:10.1007/s11894-019-0728-z (2019).
41 Imai, F. & Yoshida, Y. Molecular mechanisms underlying monosynaptic sensory-motor circuit development in the spinal cord. *Dev Dyn* **247**, 581-587, doi:10.1002/dvdy.24611 (2018).
42 Shadrach, J. L., Gomez-Frittelli, J. & Kaltschmidt, J. A. Proprioception revisited: where do we stand? *Curr Opin Physiol* **21**, 23-28, doi:10.1016/j.cophys.2021.02.003 (2021).
43 Hopkins, D. A., Bieger, D., deVente, J. & Steinbusch, W. M. Vagal efferent projections: viscerotopy, neurochemistry and effects of vagotomy. *Prog Brain Res* **107**, 79-96, doi:10.1016/s0079-6123(08)61859-2 (1996).
44 McArthur, K. L. & Fetcho, J. R. Key Features of Structural and Functional Organization of Zebrafish Facial Motor Neurons Are Resilient to Disruption of Neuronal Migration. *Curr Biol* **27**, 1746-1756 e1745, doi:10.1016/j.cub.2017.05.033 (2017).
45 Asante, E. *et al.* Defective Neuronal Positioning Correlates With Aberrant Motor Circuit Function in Zebrafish. *Front Neural Circuits* **15**, 690475, doi:10.3389/fncir.2021.690475 (2021).
46 Williams, E. K. *et al.* Sensory Neurons that Detect Stretch and Nutrients in the Digestive System. *Cell* **166**, 209-221, doi:10.1016/j.cell.2016.05.011 (2016).
47 Chang, R. B., Strochlic, D. E., Williams, E. K., Umans, B. D. & Liberles, S. D. Vagal Sensory Neuron Subtypes that Differentially Control Breathing. *Cell* **161**, 622-633, doi:10.1016/j.cell.2015.03.022 (2015).

48 da Silva, S. *et al.* Proper formation of whisker barrelettes requires periphery-derived Smad4-dependent TGF-beta signaling. *Proc Natl Acad Sci U S A* **108**, 3395-3400, doi:10.1073/pnas.1014411108 (2011).
49 Lee, L. J., Lo, F. S. & Erzurumlu, R. S. NMDA receptor-dependent regulation of axonal and dendritic branching. *J Neurosci* **25**, 2304-2311, doi:10.1523/JNEUROSCI.4902-04.2005 (2005).
50 Hebb, D. O. *The organization of behavior : a neuropsychological theory*. (Wiley, 1949).
51 Berke, B., Wittnam, J., McNeill, E., Van Vactor, D. L. & Keshishian, H. Retrograde BMP signaling at the synapse: a permissive signal for synapse maturation and activity-dependent plasticity. *J Neurosci* **33**, 17937-17950, doi:10.1523/JNEUROSCI.6075-11.2013 (2013).
52 Baines, R. A. Synaptic strengthening mediated by bone morphogenetic protein-dependent retrograde signaling in the Drosophila CNS. *J Neurosci* **24**, 6904-6911, doi:10.1523/JNEUROSCI.1978-04.2004 (2004).
53 Ito, M. Cerebellar learning in the vestibulo-ocular reflex. *Trends Cogn Sci* **2**, 313-321, doi:10.1016/s1364-6613(98)01222-4 (1998).
54 Niell, C. M., Meyer, M. P. & Smith, S. J. In vivo imaging of synapse formation on a growing dendritic arbor. *Nat Neurosci* **7**, 254-260, doi:10.1038/nn1191 (2004).
55 Finger, T. E. Sorting food from stones: the vagal taste system in Goldfish, Carassius auratus. *J Comp Physiol A Neuroethol Sens Neural Behav Physiol* **194**, 135-143, doi:10.1007/s00359-007-0276-0 (2008).
56 Travagli, R. A., Hermann, G. E., Browning, K. N. & Rogers, R. C. Brainstem circuits regulating gastric function. *Annu Rev Physiol* **68**, 279-305, doi:10.1146/annurev.physiol.68.040504.094635 (2006).
57 Ran, C., Boettcher, J. C., Kaye, J. A., Gallori, C. E. & Liberles, S. D. A brainstem map for visceral sensations. *Nature* **609**, 320-326, doi:10.1038/s41586-022-05139-5 (2022).
58 Prescott, S. L., Umans, B. D., Williams, E. K., Brust, R. D. & Liberles, S. D. An Airway Protection Program Revealed by Sweeping Genetic Control of Vagal Afferents. *Cell* **181**, 574-589 e514, doi:10.1016/j.cell.2020.03.004 (2020).
59 Polverino, M. *et al.* Anatomy and neuro-pathophysiology of the cough reflex arc. *Multidiscip Respir Med* **7**, 5, doi:10.1186/2049-6958-7-5 (2012).
60 Davey, C. F., Mathewson, A. W. & Moens, C. B. PCP Signaling between Migrating Neurons and their Planar-Polarized Neuroepithelial Environment Controls Filopodial Dynamics and Directional Migration. *PLoS Genet* **12**, e1005934, doi:10.1371/journal.pgen.1005934 (2016).
61 Grant, P. K. & Moens, C. B. The neuroepithelial basement membrane serves as a boundary and a substrate for neuron migration in the zebrafish hindbrain. *Neural Dev* **5**, 9, doi:10.1186/1749-8104-5-9 (2010).
62 Gau, P. *et al.* The zebrafish ortholog of TRPV1 is required for heat-induced locomotion. *J Neurosci* **33**, 5249-5260, doi:10.1523/JNEUROSCI.5403-12.2013 (2013).
63 Forster, D. *et al.* Genetic targeting and anatomical registration of neuronal populations in the zebrafish brain with a new set of BAC transgenic tools. *Sci Rep* **7**, 5230, doi:10.1038/s41598-017-04657-x (2017).

64 Scott, E. K. *et al.* Targeting neural circuitry in zebrafish using GAL4 enhancer trapping. *Nat Methods* **4**, 323-326, doi:10.1038/nmeth1033 (2007).
65 Muto, A. *et al.* Activation of the hypothalamic feeding centre upon visual prey detection. *Nat Commun* **8**, 15029, doi:10.1038/ncomms15029 (2017).
66 Esancy, K. *et al.* A zebrafish and mouse model for selective pruritus via direct activation of TRPA1. *Elife* **7**, doi:10.7554/eLife.32036 (2018).
67 Kimura, Y., Hisano, Y., Kawahara, A. & Higashijima, S. Efficient generation of knock-in transgenic zebrafish carrying reporter/driver genes by CRISPR/Cas9-mediated genome engineering. *Sci Rep* **4**, 6545, doi:10.1038/srep06545 (2014).
68 Giovannucci, A. *et al.* CaImAn an open source tool for scalable calcium imaging data analysis. *Elife* **8**, doi:10.7554/eLife.38173 (2019).
69 Stringer, C., Wang, T., Michaelos, M. & Pachitariu, M. Cellpose: a generalist algorithm for cellular segmentation. *Nat Methods* **18**, 100-106, doi:10.1038/s41592-020-01018-x (2021).
70 Romano, S. A. *et al.* An integrated calcium imaging processing toolbox for the analysis of neuronal population dynamics. *PLoS Comput Biol* **13**, e1005526, doi:10.1371/journal.pcbi.1005526 (2017).
71 Boulanger-Weill, J. *et al.* Functional Interactions between Newborn and Mature Neurons Leading to Integration into Established Neuronal Circuits. *Curr Biol* **27**, 1707-1720 e1705, doi:10.1016/j.cub.2017.05.029 (2017).

Figure 1

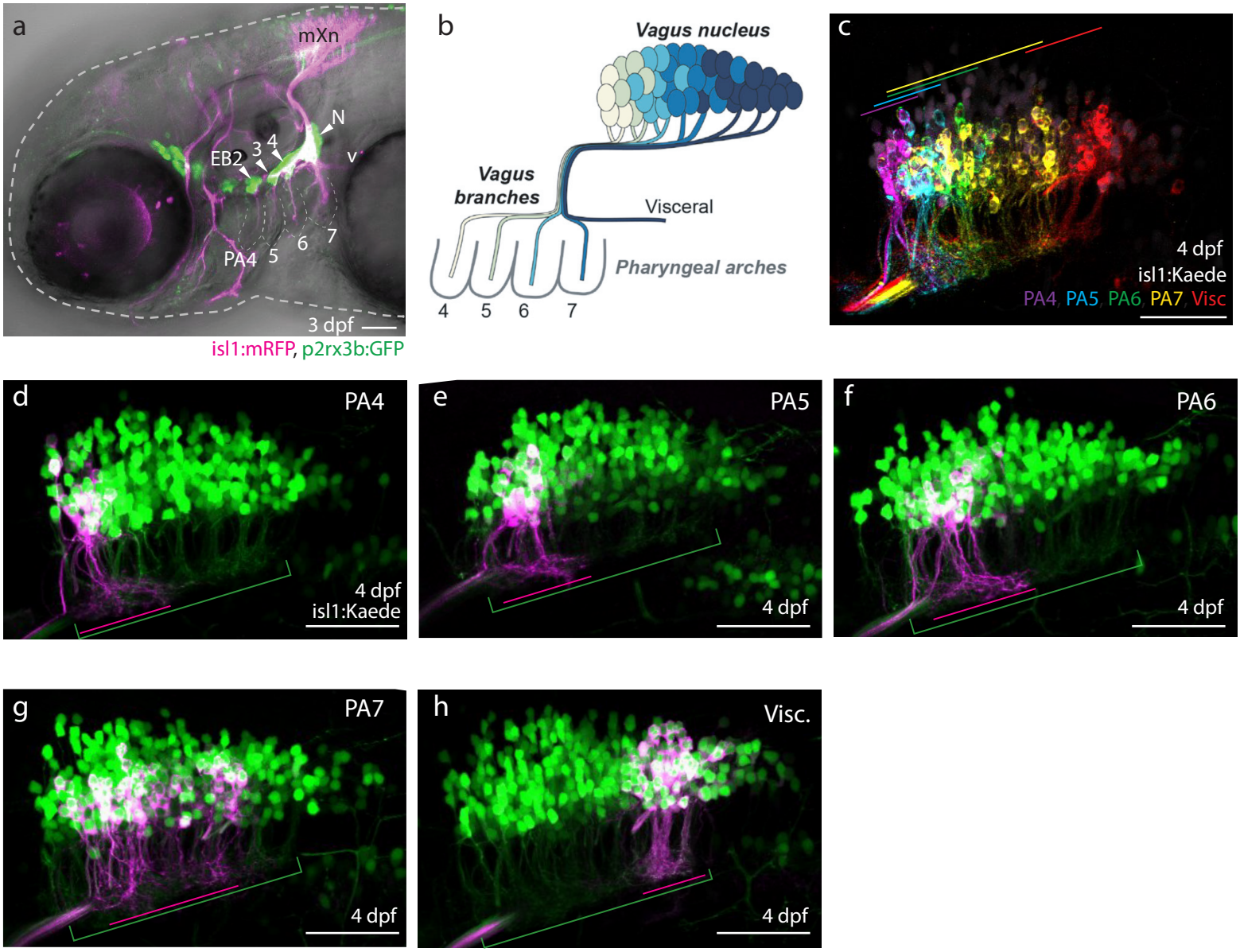
a
mXn
N
EB2
3
4
v
PA4
5
6
7
3 dpf
isl1:mRFP, p2rx3b:GFP
b
Vagus nucleus
Vagus branches
Visceral
Pharyngeal arches
4
5
6
7
c
4 dpf
isl1:Kaede
PA4, PA5, PA6, PA7, Visc
d
PA4
4 dpf
isl1:Kaede
e
PA5
4 dpf
f
PA6
4 dpf
g
PA7
4 dpf
h
Visc.
4 dpf

Figure 2

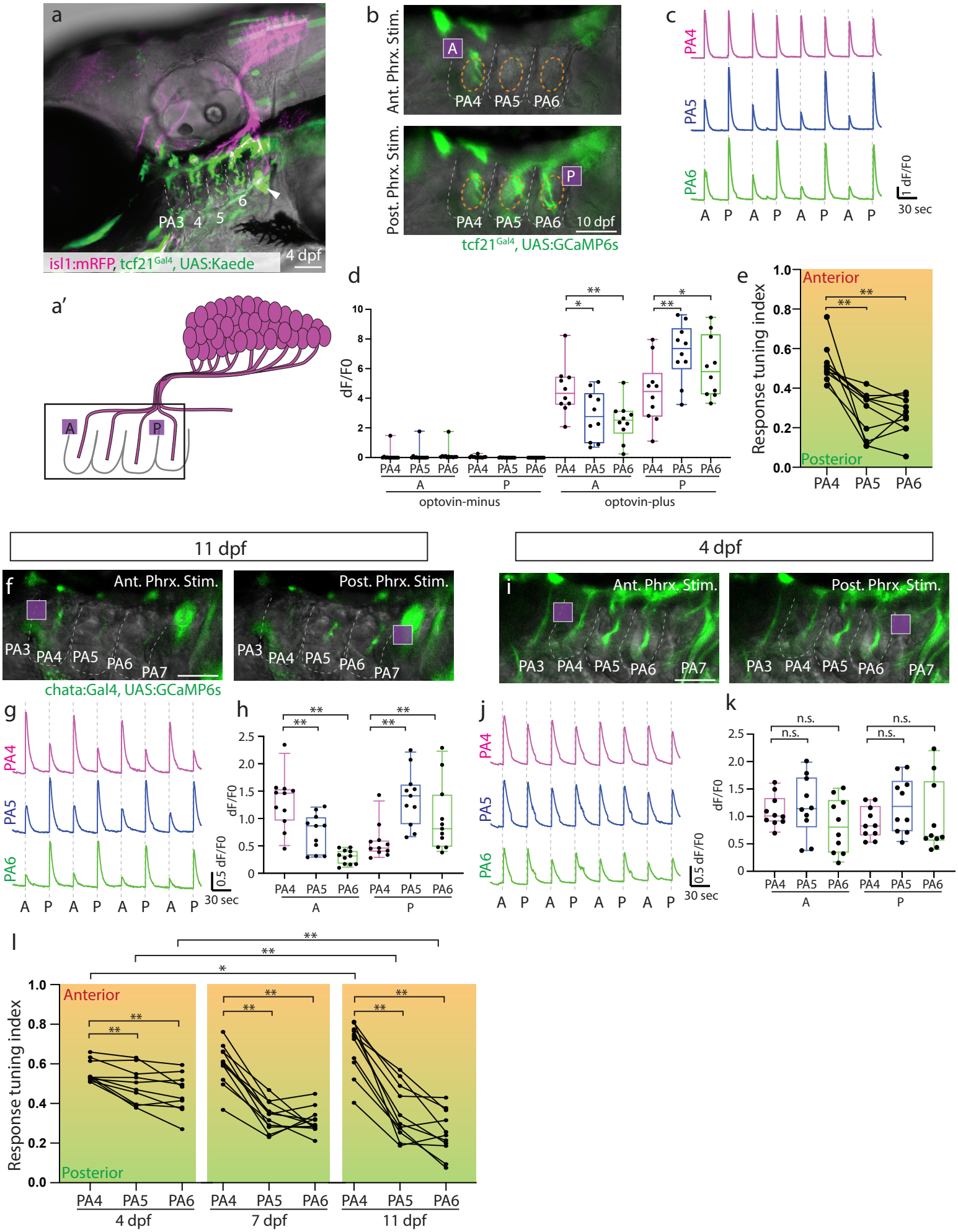
a
PA3 4 5 6
isl1:mRFP, tcf21Gal4, UAS:Kaede
4 dpf
a′
A
P
b
Ant. Phrx. Stim.
A
PA4 PA5 PA6
Post. Phrx. Stim.
P
PA4 PA5 PA6 10 dpf
tcf21Gal4, UAS:GCaMP6s
c
PA4
PA5
PA6
dF/F0
30 sec
A P A P A P A P
d
dF/F0
PA4 PA5 PA6 PA4 PA5 PA6 PA4 PA5 PA6 PA4 PA5 PA6
A P A P
optovin-minus optovin-plus
e
Anterior
Posterior
Response tuning index
PA4 PA5 PA6
11 dpf
4 dpf
f
Ant. Phrx. Stim.
Post. Phrx. Stim.
PA3 PA4 PA5 PA6 PA7
chata:Gal4, UAS:GCaMP6s
i
Ant. Phrx. Stim.
Post. Phrx. Stim.
PA3 PA4 PA5 PA6 PA7
g
PA4
PA5
PA6
0.5 dF/F0
30 sec
A P A P A P A P
h
dF/F0
PA4 PA5 PA6 PA4 PA5 PA6
A P
j
PA4
PA5
PA6
0.5 dF/F0
30 sec
A P A P A P A P
k
n.s.
dF/F0
PA4 PA5 PA6 PA4 PA5 PA6
A P
l
Anterior
Posterior
Response tuning index
PA4 PA5 PA6 PA4 PA5 PA6 PA4 PA5 PA6
4 dpf 7 dpf 11 dpf

Figure 3

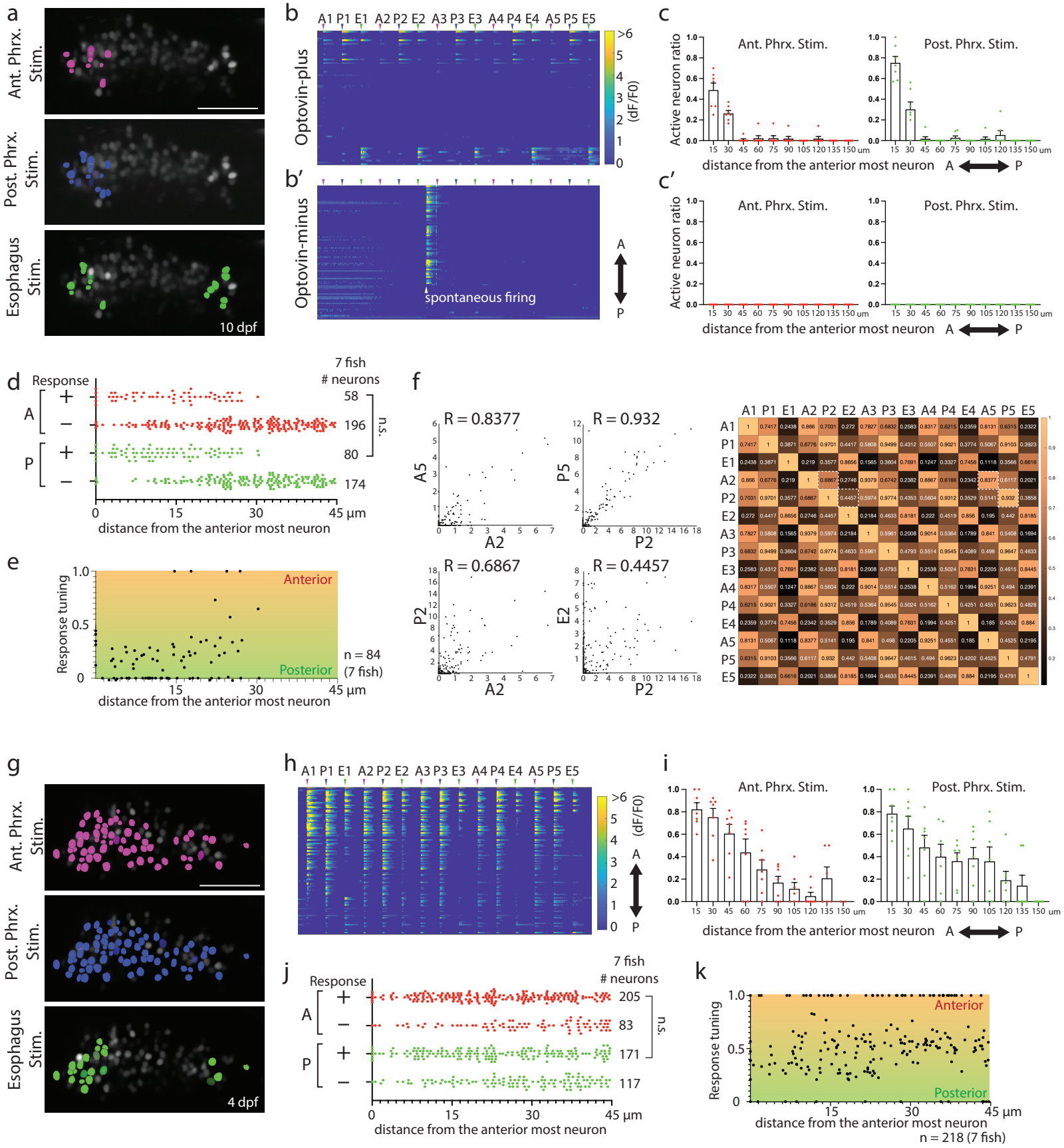
a
Ant. Phrx. Stim.
Post. Phrx. Stim.
Esophagus Stim.
10 dpf
b
A1 P1 E1 A2 P2 E2 A3 P3 E3 A4 P4 E4 A5 P5 E5
Optovin-plus
(dF/F0)
b′
Optovin-minus
spontaneous firing
A
P
c
Ant. Phrx. Stim.
Post. Phrx. Stim.
Active neuron ratio
distance from the anterior most neuron
c′
d
Response
7 fish
# neurons
58
196
80
174
n.s.
distance from the anterior most neuron
e
Anterior
Posterior
Response tuning
n = 84
(7 fish)
distance from the anterior most neuron
f
R = 0.8377
R = 0.932
R = 0.6867
R = 0.4457
A5
A2
P5
P2
E2
g
Ant. Phrx. Stim.
Post. Phrx. Stim.
Esophagus Stim.
4 dpf
h
A1 P1 E1 A2 P2 E2 A3 P3 E3 A4 P4 E4 A5 P5 E5
(dF/F0)
A
P
i
Ant. Phrx. Stim.
Post. Phrx. Stim.
distance from the anterior most neuron
j
Response
7 fish
# neurons
205
83
171
117
n.s.
distance from the anterior most neuron
k
Anterior
Posterior
Response tuning
distance from the anterior most neuron
n = 218 (7 fish)

Figure 4

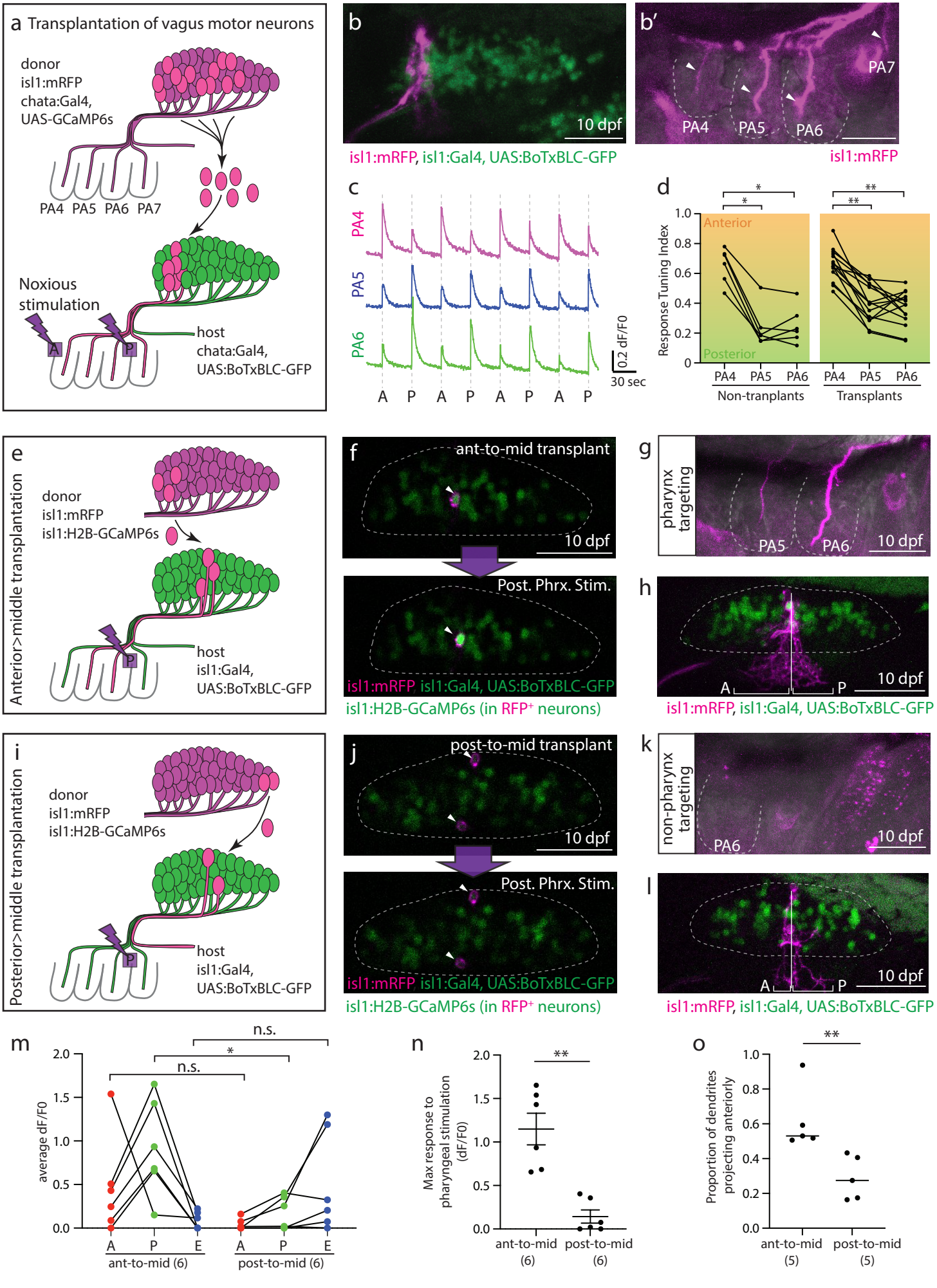
a Transplantation of vagus motor neurons
donor
isl1:mRFP
chata:Gal4,
UAS-GCaMP6s
PA4 PA5 PA6 PA7
Noxious
stimulation
A
P
host
chata:Gal4,
UAS:BoTxBLC-GFP
b
10 dpf
isl1:mRFP, isl1:Gal4, UAS:BoTxBLC-GFP
b′
PA7
PA4
PA5
PA6
isl1:mRFP
c
PA4
PA5
PA6
0.2 dF/F0
30 sec
A P A P A P A P
d
Anterior
Posterior
Response Tuning Index
PA4 PA5 PA6
Non-tranplants
PA4 PA5 PA6
Transplants
e
Anterior>middle transplantation
donor
isl1:mRFP
isl1:H2B-GCaMP6s
host
isl1:Gal4,
UAS:BoTxBLC-GFP
f
ant-to-mid transplant
10 dpf
Post. Phrx. Stim.
isl1:mRFP isl1:Gal4, UAS:BoTxBLC-GFP
isl1:H2B-GCaMP6s (in RFP+ neurons)
g
pharynx
targeting
PA5
PA6
10 dpf
h
A
P
10 dpf
isl1:mRFP, isl1:Gal4, UAS:BoTxBLC-GFP
i
Posterior>middle transplantation
donor
isl1:mRFP
isl1:H2B-GCaMP6s
host
isl1:Gal4,
UAS:BoTxBLC-GFP
j
post-to-mid transplant
10 dpf
Post. Phrx. Stim.
isl1:mRFP isl1:Gal4, UAS:BoTxBLC-GFP
isl1:H2B-GCaMP6s (in RFP+ neurons)
k
non-pharynx
targeting
PA6
10 dpf
l
A
P
10 dpf
isl1:mRFP, isl1:Gal4, UAS:BoTxBLC-GFP
m
average dF/F0
A P E A P E
ant-to-mid (6)
post-to-mid (6)
n.s.
n.s.
*
n
Max response to
pharyngeal stimulation
(dF/F0)
ant-to-mid
(6)
post-to-mid
(6)
**
o
Proportion of dendrites
projecting anteriorly
ant-to-mid
(5)
post-to-mid
(5)
**

Figure 5

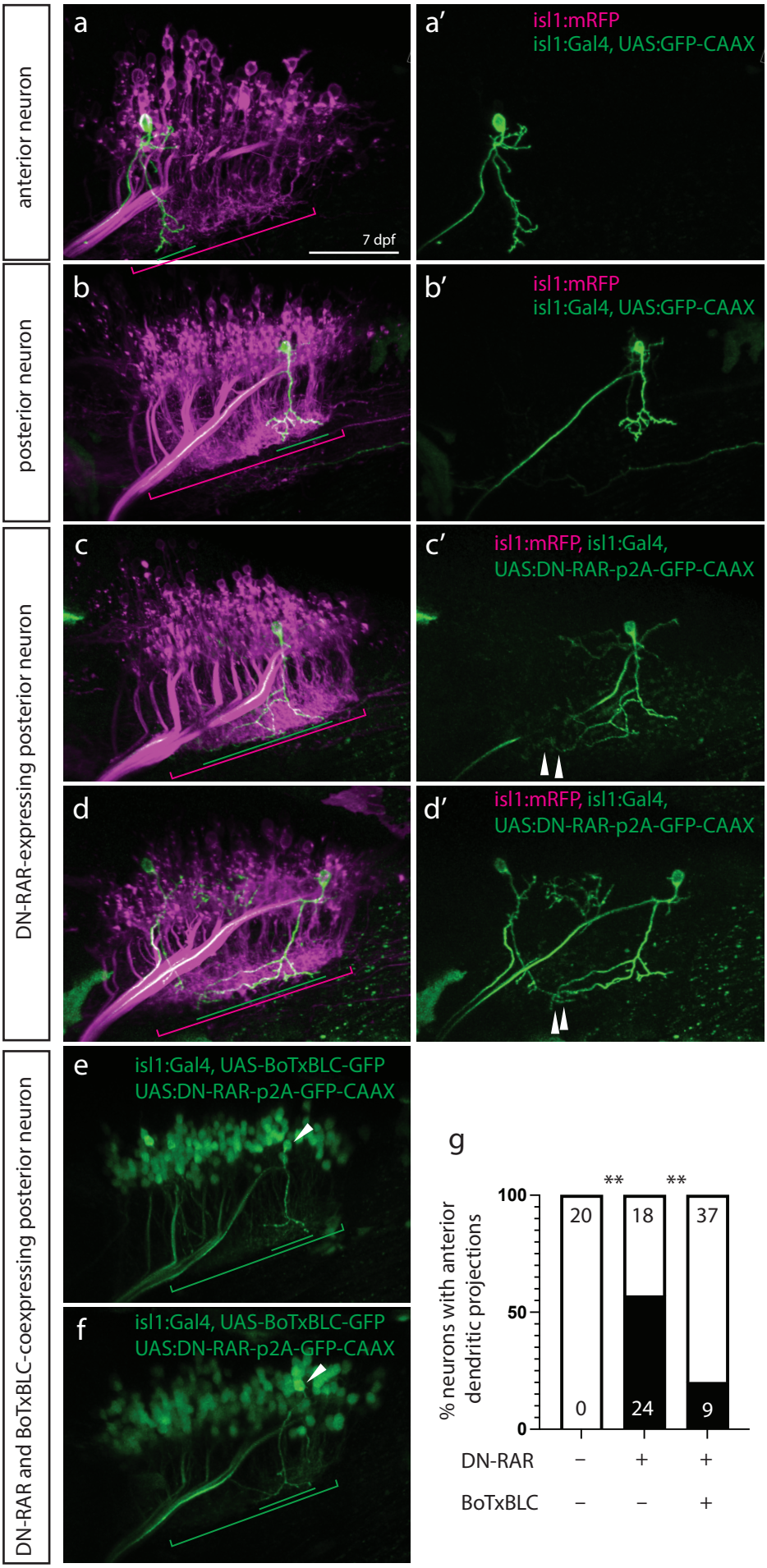
anterior neuron
posterior neuron
DN-RAR-expressing posterior neuron
DN-RAR and BoTxBLC-coexpressing posterior neuron
a
a′
isl1:mRFP
isl1:Gal4, UAS:GFP-CAAX
7 dpf
b
b′
isl1:mRFP
isl1:Gal4, UAS:GFP-CAAX
c
c′
isl1:mRFP, isl1:Gal4,
UAS:DN-RAR-p2A-GFP-CAAX
d
d′
isl1:mRFP, isl1:Gal4,
UAS:DN-RAR-p2A-GFP-CAAX
e
isl1:Gal4, UAS-BoTxBLC-GFP
UAS:DN-RAR-p2A-GFP-CAAX
f
isl1:Gal4, UAS-BoTxBLC-GFP
UAS:DN-RAR-p2A-GFP-CAAX
g
% neurons with anterior dendritic projections
100
50
0
**
**
20
0
18
24
37
9
DN-RAR − + +
BoTxBLC − − +

Figure 6

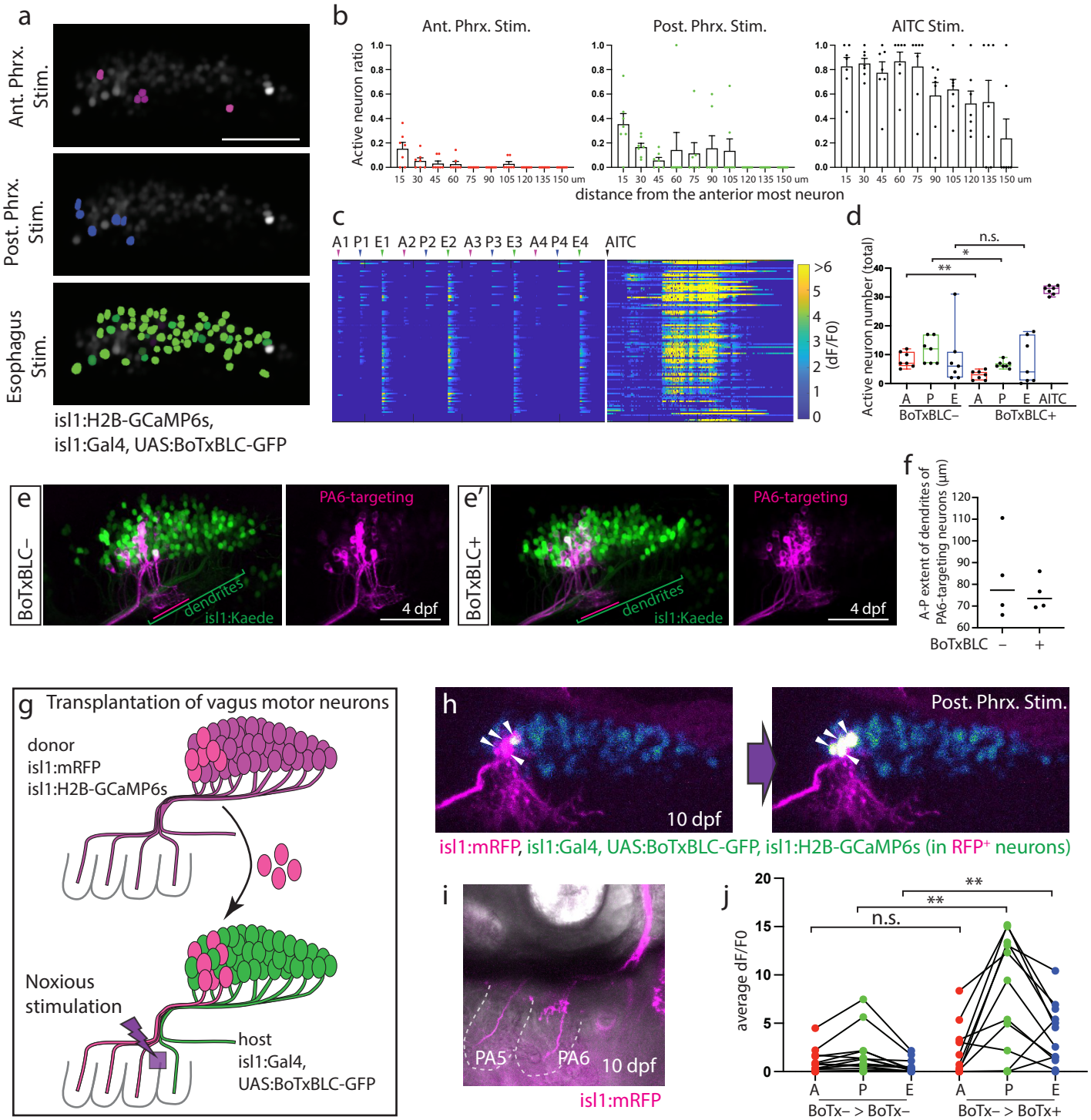
a
Ant. Phrx. Stim.
Post. Phrx. Stim.
Esophagus Stim.
isl1:H2B-GCaMP6s,
isl1:Gal4, UAS:BoTxBLC-GFP
b
Ant. Phrx. Stim.
Post. Phrx. Stim.
AITC Stim.
Active neuron ratio
distance from the anterior most neuron
c
A1 P1 E1 A2 P2 E2 A3 P3 E3 A4 P4 E4 AITC
(dF/F0)
d
Active neuron number (total)
n.s.
*
**
A P E A P E AITC
BoTxBLC– BoTxBLC+
e
BoTxBLC–
PA6-targeting
dendrites
isl1:Kaede
4 dpf
e′
BoTxBLC+
PA6-targeting
dendrites
isl1:Kaede
4 dpf
f
A-P extent of dendrites of PA6-targeting neurons (µm)
BoTxBLC – +
g Transplantation of vagus motor neurons
donor
isl1:mRFP
isl1:H2B-GCaMP6s
Noxious stimulation
host
isl1:Gal4,
UAS:BoTxBLC-GFP
h
10 dpf
Post. Phrx. Stim.
isl1:mRFP, isl1:Gal4, UAS:BoTxBLC-GFP, isl1:H2B-GCaMP6s (in RFP+ neurons)
i
PA5
PA6
10 dpf
isl1:mRFP
j
average dF/F0
n.s.
**
**
A P E A P E
BoTx– > BoTx– BoTx– > BoTx+

Figure 7

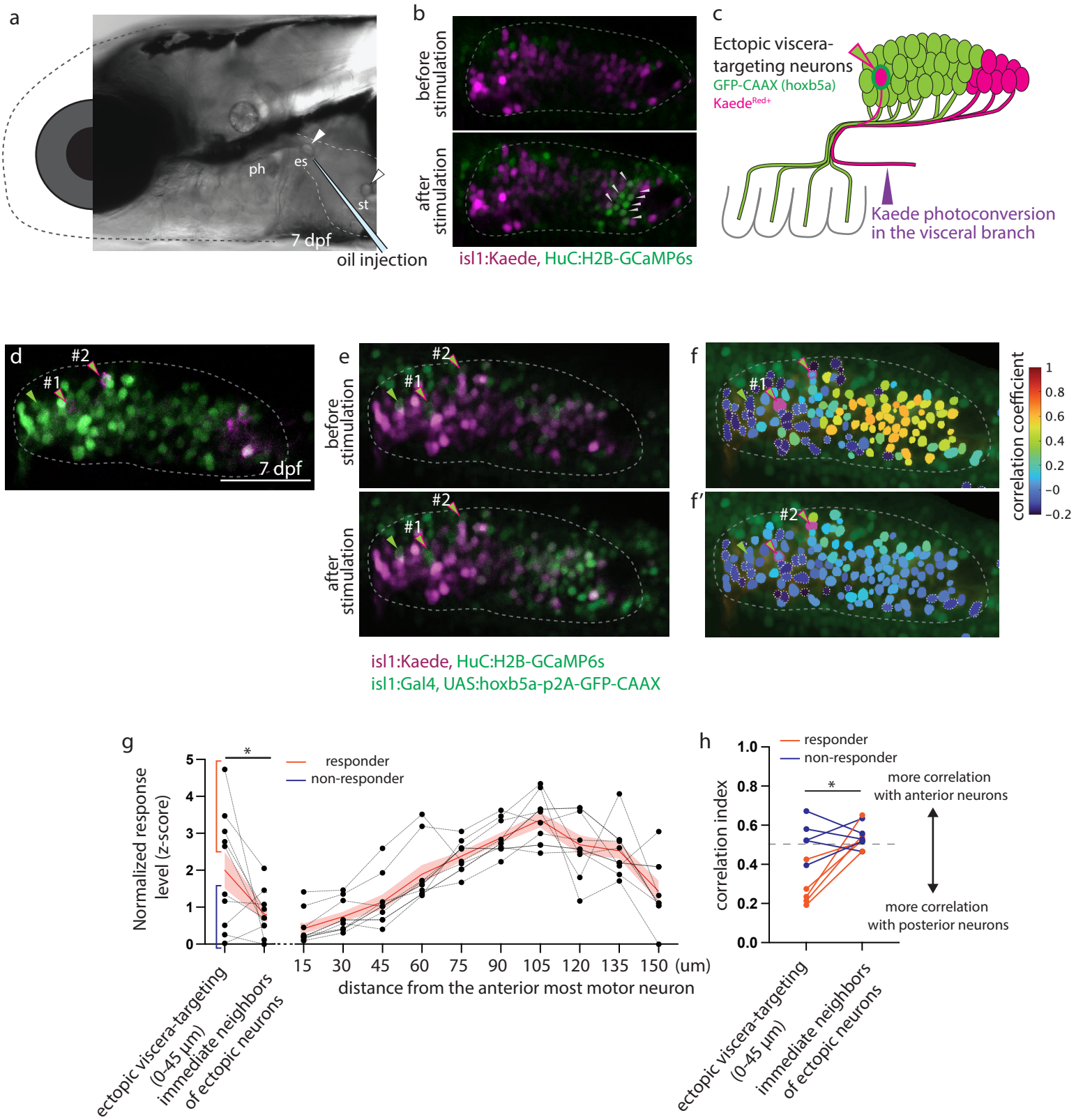
a
ph
es
st
7 dpf
oil injection
b
before stimulation
after stimulation
isl1:Kaede, HuC:H2B-GCaMP6s
c
Ectopic viscera-targeting neurons
GFP-CAAX (hoxb5a)
Kaede^Red+
Kaede photoconversion in the visceral branch
d
#1
#2
7 dpf
e
before stimulation
after stimulation
f
f'
correlation coefficient
1
0.8
0.6
0.4
0.2
−0
−0.2
isl1:Kaede, HuC:H2B-GCaMP6s
isl1:Gal4, UAS:hoxb5a-p2A-GFP-CAAX
g
Normalized response level (z-score)
responder
non-responder
*
distance from the anterior most motor neuron
15 30 45 60 75 90 105 120 135 150 (um)
ectopic viscera-targeting (0-45 µm)
immediate neighbors of ectopic neurons
h
correlation index
more correlation with anterior neurons
more correlation with posterior neurons

Figure S1

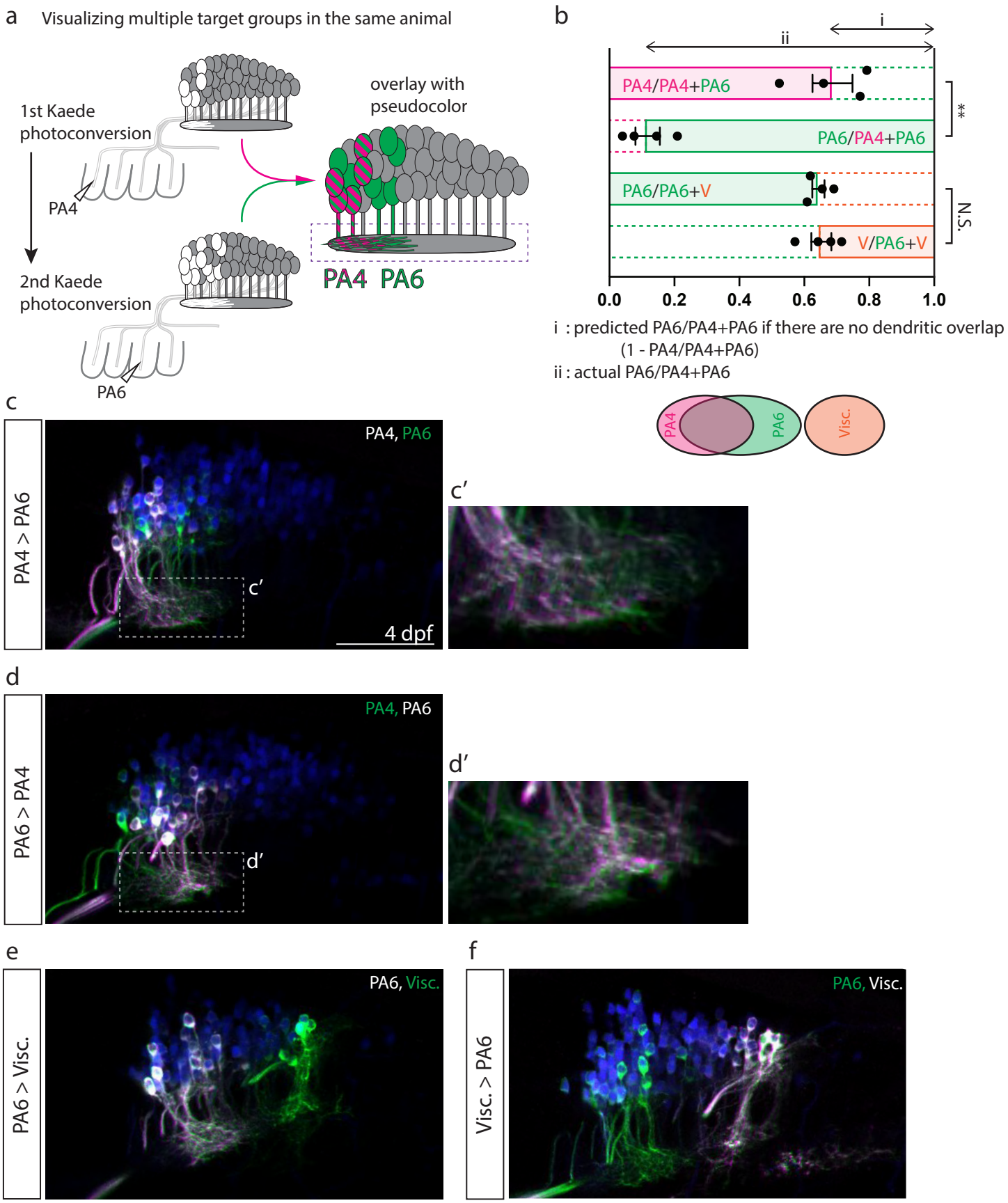
a
Visualizing multiple target groups in the same animal
1st Kaede photoconversion
PA4
2nd Kaede photoconversion
PA6
overlay with pseudocolor
PA4 PA6
b
i
ii
PA4/PA4+PA6
PA6/PA4+PA6
PA6/PA6+V
V/PA6+V
**
N.S.
0.0
0.2
0.4
0.6
0.8
1.0
i : predicted PA6/PA4+PA6 if there are no dendritic overlap
(1 - PA4/PA4+PA6)
ii : actual PA6/PA4+PA6
PA4
PA6
Visc.
c
PA4 > PA6
PA4, PA6
c′
4 dpf
c′
d
PA6 > PA4
PA4, PA6
d′
d′
e
PA6 > Visc.
PA6, Visc.
f
Visc. > PA6
PA6, Visc.

Figure S2

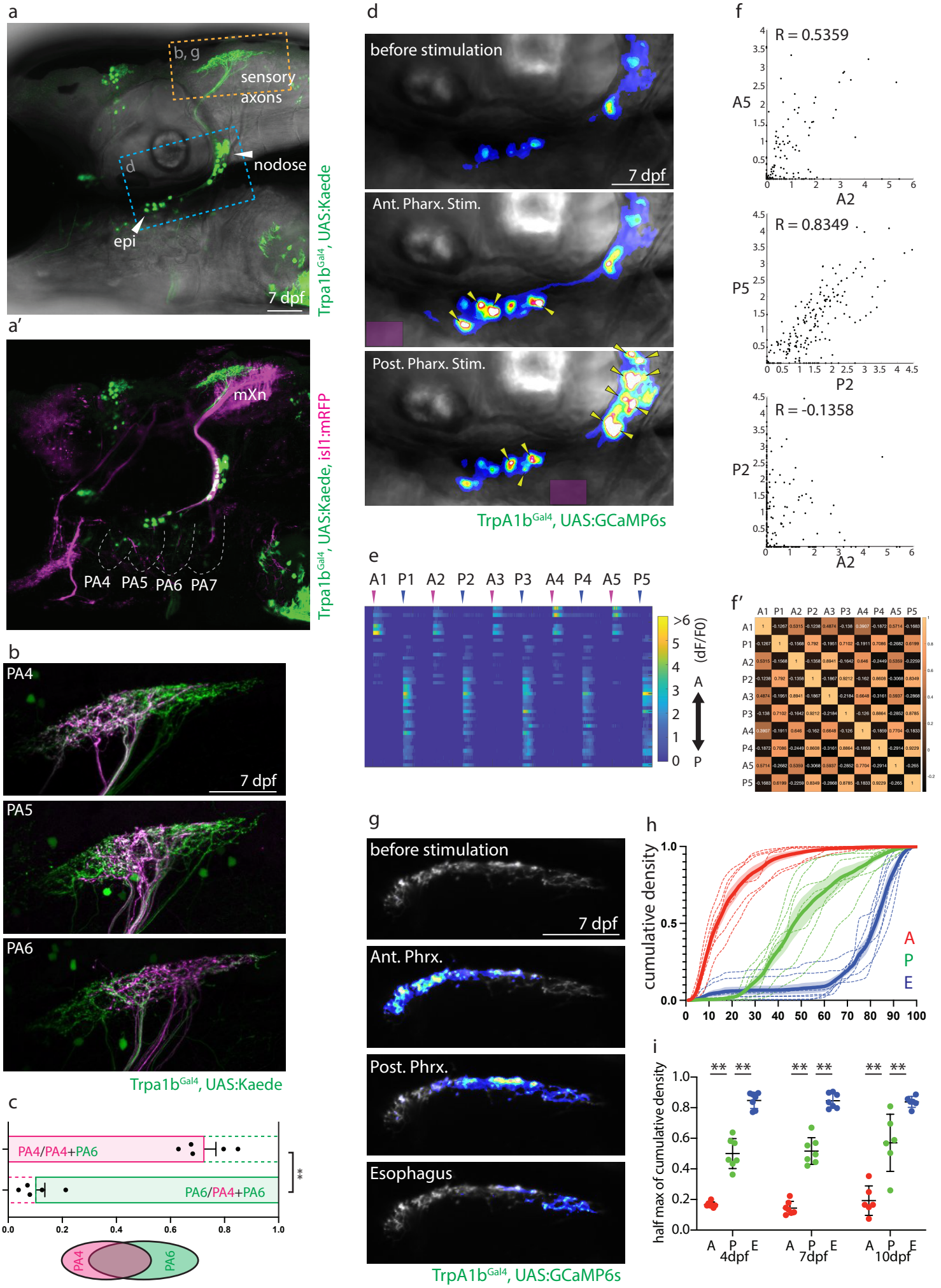
a
b, g
sensory
axons
nodose
d
epi
7 dpf
Trpa1b$^{Gal4}$, UAS:Kaede
a′
mXn
PA4 PA5 PA6 PA7
Trpa1b$^{Gal4}$, UAS:Kaede, isl1:mRFP
b
PA4
7 dpf
PA5
PA6
Trpa1b$^{Gal4}$, UAS:Kaede
c
PA4/PA4+PA6
PA6/PA4+PA6
**
0.0 0.2 0.4 0.6 0.8 1.0
PA4
PA6
d
before stimulation
7 dpf
Ant. Pharx. Stim.
Post. Pharx. Stim.
TrpA1b$^{Gal4}$, UAS:GCaMP6s
e
A1 P1 A2 P2 A3 P3 A4 P4 A5 P5
>6
5
4
3
2
1
0
(dF/F0)
A
P
f
R = 0.5359
A5
A2
R = 0.8349
P5
P2
R = -0.1358
P2
A2
f′
A1 P1 A2 P2 A3 P3 A4 P4 A5 P5
g
before stimulation
7 dpf
Ant. Phrx.
Post. Phrx.
Esophagus
TrpA1b$^{Gal4}$, UAS:GCaMP6s
h
cumulative density
1.0
0.5
0.0
0 10 20 30 40 50 60 70 80 90 100
A
P
E
i
half max of cumulative density
1.0
0.8
0.6
0.4
0.2
0.0
** **
** **
** **
A P E
4dpf
A P E
7dpf
A P E
10dpf